bioRxiv preprint doi: https://doi.org/10.1101/660662; this version posted June 5, 2019. The copyright holder for this preprint (which was not certified by peer review) is the author/funder. All rights reserved. No reuse allowed without permission.

The transcription factor Shox2 shapes thalamocortical neuron firing properties by regulation of key ion channels

Diankun Yu[1], Matthieu Maroteaux[1], Yingnan Song[2], Xiao Han[1], Isabella Febbo[1], Claire Namboodri[1], Cheng Sun[2], Wenduo Ye[2], Emily Meyer[1], Stuart Rowe[1], YP Chen[2], LA Schrader[1,2]

1. **Neuroscience Program, Brain Institute, Tulane University**
2. **Cell and Molecular Biology, Tulane University**

Running Title: Shox2 affects thalamocortical neuron function

Abstract: 256
Intro: 938
Results: 4067
Discussion: 1093
Methods: 3290

Address for LAS:
Cell and Molecular Biology
2000 Percival Stern Hall
6400 Freret St.
New Orleans, LA 70118
schrader@tulane.edu

bioRxiv preprint doi: https://doi.org/10.1101/660662; this version posted June 5, 2019. The copyright holder for this preprint (which was not certified by peer review) is the author/funder. All rights reserved. No reuse allowed without permission.

ABSTRACT

Thalamocortical neurons (TCNs) transmit information about sensory stimuli from the thalamus to the cortex and are capable of tonic and phasic burst firing modes in response to different physiological states. These firing properties of TCNs are supported by precisely-timed inhibitory synaptic inputs from the thalamic reticular nucleus and intrinsic T-type Ca^{2+} and HCN currents. These intrinsic currents are mediated by Cav3.1 and HCN channel subunits, and alterations in expression or these channels can have dramatic implications on thalamus function. The factors that modulate these currents controlling the firing patterns important for integration of the sensory stimuli and the consequences resulting from the disruption of these firing patterns are not well understood. Shox2 is a transcription factor important for pacemaker activity in the heart that is also expressed in adult mouse thalamus. We hypothesized that genes regulated by Shox2's transcriptional activity may be important for firing properties of TCNs. In this study, we used RNA sequencing on control and *Shox2* knockout mice to determine *Shox2*-affected genes and revealed a network of ion channel genes important for neuronal firing properties. Quantitative PCR confirmed that expression of *Hcn*2, 4 and Cav3.1 genes were affected by *Shox2* KO. Western blotting showed expression of the proteins for these channels was decreased in the thalamus, and electrophysiological recordings showed that Shox2 KO impacted the firing properties of a subpopulation of TCNs. Finally, behavioral studies revealed that *Shox2* expression in TCNs play a role in somatosensory function and object memory. Overall, these results reveal Shox2 as a transcription factor important for TCN function.

INTRODUCTION

Processing of sensory information is mediated by precise circuitry that senses stimuli in the periphery and transforms the information through a network of synaptic connections to ultimately allow perception and cognitive processing of the surrounding world. Rhythmic oscillations of brain activity crucial to cognitive function emerge from neuronal network interactions that consist of reciprocal connections between the thalamus, the inhibitory thalamic reticular nucleus and the cortex [1]. Dysfunction of these oscillations caused by aberrant activity in the thalamic circuit is thought to play a role in many neuropathological

bioRxiv preprint doi: https://doi.org/10.1101/660662; this version posted June 5, 2019. The copyright holder for this preprint (which was not certified by peer review) is the author/funder. All rights reserved. No reuse allowed without permission.

conditions, including epilepsy [2-4], autism [5-7], and schizophrenia [8-11]. Furthermore, damage to thalamic nuclei, especially medial and anterior nuclei, causes severe memory deficits known as diencephalic amnesia [12-17].

The intrinsic properties that shape action potential firing and contribute to rhythmic oscillations of the thalamocortical neurons (TCNs) are important for efficient transfer of information from the thalamus to the cortex. Notably, TCNs switch their firing states between 2 modes, burst and tonic firing modes [18-20]. The transitions between tonic and burst modes are controlled by voltage-gated currents within the TCNs, mainly T-type Ca^{2+} currents (I_T) and H-currents (I_h), mediated by Cav3.x and HCN family of channels, respectively [1]. Interplay of the kinetics of these currents can establish a cycle of oscillatory activity that generates rhythmic activity in the thalamocortical network [21]. Consequently, modulation of I_T and I_h in TCNs is an important regulatory mechanism of firing activity crucial for sensory perception, sleep activity and cognition. Very little is understood about the factors that contribute to modulation of the ion channels that underlie these currents.

The transcription factor, Shox2, represents a possible mechanism to coordinate expression of the ion channels important for TCN firing properties. Shox2 is a member of the homeobox family of transcription factors [22-24], and recent studies suggest it is important for development and maintenance of rhythmic activity in adult heart. Cells in the sinoatrial node of the heart generate spontaneous, rhythmic action potentials and lead other working myocytes to beat at a stable firing rate, thus these cells are known as pacemaker cells [25]. The rhythmic action potential generation in the pacemaker cells is mediated by the prominent expression of HCN channels and T-type calcium channels [26, 27]. We and others have shown that *Shox2* plays a decisive role in the differentiation of pacemaker cells in the sinoatrial node of the heart and pulmonary vein in mice, and Shox2 expression in the SAN is necessary for

bioRxiv preprint doi: https://doi.org/10.1101/660662; this version posted June 5, 2019. The copyright holder for this preprint (which was not certified by peer review) is the author/funder. All rights reserved. No reuse allowed without permission.

cardiac pacemaker-type activity [28, 29]. Importantly, Shox2 is essential for expression of HCN4 channels [28], and *Shox2* overexpression favors differentiation of mouse embryonic stem cells into pacemaker cells with biological pacing ability and enhanced HCN currents [30]. *Shox2* expression in the sinoatrial node of the heart continues into adulthood since cells of the sinoatrial node maintain pacemaker properties. However, *Shox2* expression is suppressed in pulmonary vein and coronary sinus in the adult, and these cells lose pacemaker properties during development [31]. These results suggest that Shox2 expression is critical for expression of channels important for myocyte firing properties and is a determinant of pacemaker properties of the sinoatrial node.

During development of the nervous system, *Shox2* expression has been reported in neurons of the facial motor nucleus (nVII) [32], cerebellum [33], spinal cord [34] and dorsal root ganglia [35]. *Shox2*-expressing excitatory interneurons in the ventral spinal cord are rhythmically active during locomotor-like activity, and synaptic and electrical connections between Shox2-expressing interneurons are crucial for the frequency and stability of their rhythmic activity [34, 36], suggesting that interconnectivity between *Shox2*-expressing neurons is critical for synchronization of rhythmic activity. These results suggest that *Shox2*-expressing neurons play a critical role in central pattern generation important for locomotion, but the role of *Shox2* in this rhythmic behavior was not further investigated.

In this study, we found that *Shox2* is expressed in thalamocortical neurons (TCNs) in adult mice. TCNs express HCN2, HCN4 and $Ca_v3.1$ channel protein subunits that are important for firing properties of TCNs, and we hypothesized that *Shox2* also coordinates the expression of genes for these ion channels to affect action potential firing activity of TCNs. Using conditional KO animals, we further demonstrated that *Shox2* is important for firing properties, including spike frequency, delay and resonance in TCNs, likely by affecting expression of mRNA of

bioRxiv preprint doi: https://doi.org/10.1101/660662; this version posted June 5, 2019. The copyright holder for this preprint (which was not certified by peer review) is the author/funder. All rights reserved. No reuse allowed without permission.

multiple ion channels, including $Ca_v3.1$, and HCN2 and HCN4. We also demonstrated that an inducible global knock-out of *Shox2* reduced anxiety behavior in the open field, impaired sensorimotor function and object recognition memory. Object memory deficits were confirmed with an inducible Shox2 knock-out in medial thalamus. The present study provides novel insight into the molecular markers that contribute to thalamocortical neuron function and shows that S*hox2* expression is critical to maintain thalamic neuron function and physiological properties by regulating gene expression in the neurons of the adult mouse thalamus.

bioRxiv preprint doi: https://doi.org/10.1101/660662; this version posted June 5, 2019. The copyright holder for this preprint (which was not certified by peer review) is the author/funder. All rights reserved. No reuse allowed without permission.

Methods

Mice

All animal procedures were approved by Tulane University Institutional Animal Care and Use Committee (IACUC) according to National Institutes of Health (NIH) guidelines. *Shox2* transgenic mice including *Shox2*^{Cre}, *Shox2*^{LacZ}, *Shox2*$^{f/f}$ and *Rosa26*^{CreERt} mice were generously donated by Dr. Yiping Chen. All wildtype C57Bl/6N mice were ordered from Charles River. *Rosa26*$^{LacZ/+}$ *(stock #003474) and Gbx2*$^{CreERt/+}$ breeders (stock #022135) were ordered from Jackson Lab.

In inducible KO experiments, *Rosa26*$^{CreERt/+}$,*Shox2*$^{f/f}$ or *Rosa26*$^{CreERt/CreERt}$,*Shox2*$^{f/f}$ female mice were crossed with *Shox2*$^{-/+}$ male mice or, in the case of the *Gbx2* animals, *Gbx2*$^{CreERt/+}$,*Shox*$^{f/f}$ or *Gbx2*$^{CreErt/CreErt}$,*Shox*$^{f/f}$ were crossed with *Shox2*$^{-/+}$ male mice (Supplemental Fig. 1). Litters were labelled and genotyped at postnatal day 10 (P10). The KO group was the *Rosa26*$^{CreERt/+}$, *Shox2*$^{-/f}$ mice (*Gbx2*$^{CreRt/+}$, *Shox2*$^{-/f}$) and the control (CR) group was the littermate *Rosa26*$^{CreERt/+}$ *(Gbx2*$^{CreErt/+}$*),Shox2*$^{+/f}$. In the *Shox2*$^{LacZ/+}$ and *Shox2*$^{Cre/+}$ mice, the first two exons of the *Shox2* allele were partially replaced by *LacZ* and *Cre* genes respectively in order to obtain the expression of *LacZ* mRNA and *Cre* mRNA under the control of the *Shox2* promoter, while the unaffected alleles express *Shox2* mRNA [24]. The *Rosa26*$^{CreERt/+}$ mouse line is a transgenic mouse line with a tamoxifen-inducible Cre^{ERt} inserted in the *Rosa26* loci. The *Rosa26*$^{LacZ/+}$ mouse line is a transgenic mouse line with a floxed stop signals followed by LacZ gene inserted in the *Rosa26* loci [37]. This 'cre reporter' mouse strain was used to test the expression of the *Cre* transgene under the regulation of a specific promoter.

The Rosa26^{CreErt} is a global KO, whereas the *Gbx2*^{CreERt} mouse was used to knockdown *Shox2* specifically in the medial thalamus. Our localization studies with *Gbx2*-promotor driven GFP staining showed that *Gbx2* promotor-driven *CreERt* is specifically expressed in the midline

bioRxiv preprint doi: https://doi.org/10.1101/660662; this version posted June 5, 2019. The copyright holder for this preprint (which was not certified by peer review) is the author/funder. All rights reserved. No reuse allowed without permission.

thalamus of the Gbx2^{CreErt} adult mouse (Supplemental Fig. 2A). Further testing using RT-qPCR showed that *Shox2* mRNA was reduced in the medial thalamus of the *Gbx2$^{CreRt/+}$, Shox2$^{-/f}$* compared to CR mice, but not lateral thalamus (Supplemental Fig. 2B).

To induce recombination in animals bearing a Cre^{ERT2}, pre-warmed tamoxifen (100-160 mg/kg) was injected intraperitoneally into KO mice and CR littermates at the same time every day for five consecutive days. Tamoxifen (20 mg/mL) was dissolved in sterile corn oil (Sigma, C8267) with 10% alcohol. The littermate KO mice and CR mice of the same sex were housed together and received the same handling. Throughout experiments, the researchers were blinded to the genotype. RT-qPCR experiments were used to confirm the efficiency of *Shox2* KO in brains in every animal tested.

In order to view projections of *Shox2*-expressing neurons, we created the Ai27D-*Shox2Cre* mouse. B6.Cg-Gt(ROSA)26Sortm27.1(CAG-COP4*H134R/tdTomato)Hze/J(Ai27D) mice from Jackson labs were crossed with *Shox2*Cre to obtain mice with Shox2-expressing neurons labeled with tdTomato and expressing ChR2 (figure 2 M-O).

X-gal staining

Adult *Shox2$^{LacZ/+}$* or *Shox2$^{Cre/+}$*, *Rosa26$^{LacZ/+}$* male mice were anaesthetized by isoflurane inhalation, decapitated, and the brains were removed. Brains were sliced at 200 µm using a Vibratome Series 3000 Plus Tissue Sectioning system. Brain slices were placed into ice-cold artificial cerebrospinal fluid (aCSF) in a 24-well plate and fixed with 0.5% glutaraldehyde and 4% paraformaldehyde in phosphate buffered saline (PBS) for 15 minutes. After 3X wash with ice-cold PBS, the slices were incubated with X-gal staining solution, containing: (X-gal (1mg/ml), potassium ferrocyanide (4 mM), potassium ferrcyanide (4mM) and $MgCl_2$(2 mM) and covered by aluminum foil at 37 °C overnight. All slices were washed and post-fixed. Images were taken under a stereo microscope.

bioRxiv preprint doi: https://doi.org/10.1101/660662; this version posted June 5, 2019. The copyright holder for this preprint (which was not certified by peer review) is the author/funder. All rights reserved. No reuse allowed without permission.

Immunohistochemistry (IHC)

Mice were deeply anaesthetized by injection with ketamine (80 mg/kg) mixed with xylazine (10 mg/kg), perfused transcardially with ice-cold phosphate-buffered saline (PBS) followed by 4% paraformaldehyde in PBS and decapitated for brain collection. Mouse brains were placed in 4% paraformaldehyde in PBS at 4 °C overnight for post-fixation. In order to perform cryostat sections, the brains were sequentially placed in 15% and 30% sucrose in PBS solutions at 4 °C until saturation. The brain samples were embedded with optimal cutting temperature compound (OCT) and stored at -20 °C and cryo-sectioned in 20-50 µm coronal slices with Leica CM3050S cryostat. For IF staining, slices were washed with 50 mM Tris Buffered Saline with 0.025% Triton X-100 (TTBS) and blocked in 2% Bovine Serum Albumin (BSA) in TTBS for 2 hours at room temperature. Primary antibodies were diluted in blocking solutions and applied on slides overnight at 4°C. Fluorescence-conjugated secondary antibodies were diluted 1:1000 in blocking solutions and applied on slides for one hour at room temperature. 1:1000 DAPI was applied for 5 minutes at room temperature for nuclei staining and washed. The slices were mounted on slides with mounting media (Vector Laboratories, H-1000) and imaged under confocal microscope.

mRNA Sequencing

Thalamus mRNA was extracted from 3 KO mice and 3 CR mice and sent to *BGI Americas Corporation (Cambridge, MA, USA)* for RNA-seq quantification. Total RNA was isolated in tissue from the midline of the thalamus of P60 male *Gbx2*$^{CreERt/+}$, *Shox2*$^{-/f}$ mice and control male littermates (*Gbx2*$^{CreERt/+}$, *Shox2*$^{+/f}$) with the same method used for RT-qPCR RNA extraction. Around 30 million single-end 50-bp reads by BGISEQ-500 Sequencing Platform per sample were aligned to the mm10/GRCm38 mouse reference genome using Salmon v0.10.2 [38]. The count data from Salmon v0.10.2 was analyzed via DESeq2 v 1.22.2 [39] to identify genes

bioRxiv preprint doi: https://doi.org/10.1101/660662; this version posted June 5, 2019. The copyright holder for this preprint (which was not certified by peer review) is the author/funder. All rights reserved. No reuse allowed without permission.

differently expressed (DEGs) between KO and CR and to calculate Fragments Per Kilobase Million (FPKMs). Genes with adjusted p value < 0.1 were defined as DEGs and were used for further gene ontology (GO) analysis through online DAVID Bioinformatics Resources [40, 41].

Quantitative reverse transcription PCR (RT-qPCR)

The whole thalamus was collected from adult mouse brains (*Rosa*^{CreErt}-*Shox2* KO) and immediately stored in RNAlater™ RNA stabilization reagent (ThermoFisher Scientific, AM7021). RNA was extracted using RNeasy Mini Kit (Qiagen, 74104) following the standard protocol provided in the manual. The RNA concentration and quality were tested using Nanodrop Microvolume Spectrophotometers and Fluorometer as well as agarose gel investigation. Reverse transcription was conducted using iScript™ Reverse Transcription Supermix (Bio- Rad, 1708840). Quantitative PCR was conducted with iTaq™ Universal SYBR Green Supermix (Bio-rad, 1725121) in Bio-Rad CFX96 Touch™ PCR system. Data analysis was done with CFX Manager software. The expression of all the genes tested in the RT-qPCR experiments were normalized to the widely used housekeeping reference gene β-actin (*Actb*) and TATA-box binding protein (*Tbp*) [42, 43]. All primers were designed and tested, and conditions were optimized to have an efficiency between 95% and 105%. Both the melt curves and gel investigations were used to confirm the RT-qPCR products. The primer sequences of all tested genes including reference gene *Actb* and *Tbp* are listed in Table 1.

To confirm knock-down of *Shox2* in the Gbx2$^{CreERt/+}$ animals, adult *Gbx2*$^{CreERt/+}$*; Shox2* $^{-/f}$ male and female mice were anaesthetized by isoflurane inhalation followed decapitation. The brains were removed and a 1 mm thick slice through the thalamus was removed via razor blade, the location of cut is determined by Paxinos and Franklin Mouse Brain Atlas. Medial thalamus tissue is collected with 1mm stainless steel punching tool and lateral thalamus was separated via razor blade. The collected tissues were stored in 50 µL RNA later solution and

bioRxiv preprint doi: https://doi.org/10.1101/660662; this version posted June 5, 2019. The copyright holder for this preprint (which was not certified by peer review) is the author/funder. All rights reserved. No reuse allowed without permission.

stored in -80 freezer. To homogenize collected tissues, 350 µL of RLT lysis buffer from Qiagen RNeasy Mini Kit is added to the tissue and homogenized with a pestle mortar. The homogenized tissues went through sonication with a Q55 sonicator (Qsonica) and then 350 µL cold, 70% EtoH was added to the sample. After this, the mixed solution is processed by series of spin and wash follow the instructions book from Qiagen RNeasy Mini Kit. Once RNAs are isolated from tissues, we applied qRT-PCR with Shox2 primer (Table 1) and normalized with GAPDH.

Table 1. Sequences of RT-qPCR primers

Gene	Forward Primer(5'->3')	Reverse Primer (5'->3')
Shox2	CCGAGTACAGGTTTGGTTTC	GGCATCCTTAAAGCACCTAC
actb	CTAGACTTCGAGCAGGAGAT	GATGCCACAGGATTCCATAC
Tbp	CCGTGAATCTTGGCTGTAAACTTG	GTTGTCCGTGGCTCTCTTATTCTC
Hcn1	CTTCGTATCGTGAGGTTTAC	GTCATAGGTCATGTGGAATATC
Hcn2	CTTTGAGACTGTGGCTATTG	GCATTCTCCTGGTTGTTG
Hcn4	ATACTTATTGCCGCCTCTAC	TGGAGTTCTTCTTGCCTATG
Cacna1g	GACACCAGGAACATCACTAAC	CACAAACAGGGACATCAGAG
Cacna1h	TTTGGGAACTATGTGCTCTTC	TCTAGGTGGGTAGATGTCTTATC
Gapdh	GTCGGTGTGAACGGATTTG	TAGACTCCACGACATACTCAGCA.

Western Blot

Thalamic tissues were collected from the adult mouse brains and immediately placed on dry ice and stored at -80 °C until use. The thalamus samples were lysed with RIPA lysis buffer (150 mM Sodium chloride, 1% Triton X-100, 0.5% sodium deoxycholate, 0.1% SDS, 50

bioRxiv preprint doi: https://doi.org/10.1101/660662; this version posted June 5, 2019. The copyright holder for this preprint (which was not certified by peer review) is the author/funder. All rights reserved. No reuse allowed without permission.

mM Tris, pH 8.0) with fresh added Halt™ protease inhibitor cocktail (ThermoFisher Scientific, 78430). Samples were centrifuged at 12,000 rpm at 4 °C for 20 minutes and the supernatant protein samples were collected. The protein concentration of the samples was determined using the Bio-Rad DC protein assay (Bio-Rad, 500-0116). Samples were normalized with the same lysis buffer, aliquoted and stored at -80°C until use. Before loading, 5X sample buffer (ThermoFisher Scientific, 39001) and dithiothreitol (final concentration - 50 mM, DTT) were added to each protein sample. Sample mixtures were left at room temperature for 30 minutes. Protein (20-30 µg/well) was loaded in a SDS-PAGE gel (4% stacking gel and 8% separating gel), together with 3 µL prestained protein ladder (ThermoFisher Scientific, 26619). The gels were run at 70 mV for 3 hours, and the proteins were transferred to a pre-activated PVDF membrane (Millipore, IPFL00005) at -70 mV for 3 to 4 hours. Sodium dodecyl sulfate (SDS) and methanol were added into transfer buffer at a final concentration of 0.1% and 10%, respectively. The gels were stained with Coomassie Brilliant Blue solution (0.1% Coomassie Brilliant Blue, 50% methanol, 10% Glacial acetic acid) to check that no obvious proteins remained under these transfer conditions. Membranes were incubated in blocking solution with 5% non-fat dry milk and 3% BSA in TTBS at room temperature for one hour. Primary antibody was diluted in Odyssey® Blocking Buffer in TBS and applied on the membrane at 4 °C overnight. After washing the membrane with TTBS, fluorescence-conjugated secondary antibodies were diluted and applied on the membrane at room temperature for one hour. Imaging of the stained membrane was done in an Odyssey CLx Infrared Scanner and analyzed by Image Studio Lite Ver 5.2.

bioRxiv preprint doi: https://doi.org/10.1101/660662; this version posted June 5, 2019. The copyright holder for this preprint (which was not certified by peer review) is the author/funder. All rights reserved. No reuse allowed without permission.

Antibodies used in IHC and Western blot experiment

Reagent/Resource	Supplier	Details
Chicken anti-β-galactosidase	Abcam	Ab9361; 1:500
Rabbit anti-NeuN Cy3- conjugated	Millipore Sigma	ABN78; 1:500
Mouse anti-parvalbumin	Millipore Sigma	MAB1572; 1:500
Rabbit-anti GFAP	PhosphoSolution	620-GFAP; 1:300
Rabbit-anti GFP	Novus Biologicals	NB 600-308; 1:300
Alexa-Fluor 488 Goat anti-mouse	Life Technologies	1:1000
Alexa-Fluor 647 Goat anti-chicken	Life Technologies	1:1000
Alexa-Fluor 594 Goat anti-rabbit	Life Technologies	1:1000
mouse anti-HCN2	Neuromab	N71/37; 1:1000
mouse anti-HCN4	Neuromab	N114/10; 1:1000
mouse anti-Cav3.1	Neuromab	N178A/9; 1:1000
IRDye 680RD Goat anti-mouse	Li-Cor	P/N 926-68070; 1:10,000
IRDye 800CW Goat anti-rabbit IgG (H+L)	Li-Cor	P/N 926-32211; 1:10,000

Electrophysiology

At the same time of the day (11:00 am summer and 10:00 am winter), mice were anaesthetized with isoflurane and decapitated. Brains were quickly removed and immersed in oxygenated (95% O_2 and 5% CO_2), ice-cold N-methyl-D-glucamine (NMDG)-based slicing solution (in mM, 110 NMDG, 110 HCl, 3 KCl, 1.1 NaH_2PO_4, 25 $NaHCO_3$, 25 Glucose, 10 ascorbic acid, 3 pyruvic acid, 10 $MgSO_4$, 0.5 $CaCl_2$). The first 350 µM coronal brain section containing the most anterior paraventricular thalamus (PVA) was obtained with a Vibratome Series 3000 Plus Tissue Sectioning System. The collected brain slices were transferred and incubated in oxygenated standard aCSF (in mM, 125 NaCl, 2.5 KCl, 26 $NaHCO_3$, 1.24 NaH_2PO_4, 25 Dextrose, 2 $MgSO_4$, 2 $CaCl_2$) at 37 °C for 30 minutes, then incubated at room temperature until use.

bioRxiv preprint doi: https://doi.org/10.1101/660662; this version posted June 5, 2019. The copyright holder for this preprint (which was not certified by peer review) is the author/funder. All rights reserved. No reuse allowed without permission.

During the recordings, an individual slice was transferred to a recording chamber and perfused with oxygenated external solution at a speed of 1 mL/minute at room temperature at room temperature. Unless otherwise specified, standard aCSF was perfused as the external solution. For isolation of the specific currents, different pharmacological antagonists were applied in the external solution as stated in the results. PVA was identified as the nucleus near the border of the third ventricle enclosed by the stria medullaris. Cell-attached and whole-cell recordings were obtained using MultiClamp 700B amplifier, Digidata 1322A digitizer, and a PC running Clampex 10.3 software (Molecular Device). For cell-attached recording, glass pipettes had resistances of 2.5 – 3.5 MΩ filled with standard aCSF. Giga seals were obtained in every cell by application of a small negative pressure for spontaneous action potential recording. For intracellular whole-cell patch clamp recording, glass pipettes had resistances of 3.5 – 6 MΩ filled with internal pipette solution (in mM, 120 Kgluconate, 20 KCl, 0.2 EGTA, 10 Hepes, 4 NaCl, 4 Mg^{2+}ATP, 14 phosphocreatine, 0.3 Tris GTP (pH was adjusted to 7.2-7.25 by KOH, osmolarity was adjusted to 305-315 mOsm by sorbitol). Series resistance was monitored and only cells with series resistance less than 20 MΩ and that did not change over 15% throughout the recording were further analyzed. Spontaneous action potentials were recorded in current clamp mode at membrane potential. Cells with no action potentials identified in 5 minutes are classified as 'not active' cells.

Impedance profile analysis: The ZAP (impedance (Z) amplitude profile) current (I_{ZAP}) stimulus follows a sinusoidal function with a fixed amplitude (5pA) and sweeping frequency (0-20Hz) over 20 seconds. The function is: I_{ZAP}= 5pA* $\sin(\pi*t^2)$ where tϵ (0,20s). The ZAP current was injected in neurons held at -70mV and the voltage response (V_{ZAP}) of neurons was recorded. The impedance frequency profile (Z(f)) was obtained from the ratio of Fast Fourier Transforms (FFT) of V_{ZAP} and FFT of I_{ZAP} ($Z(f)=fft(V_{ZAP})/fft(I_{ZAP})$. The magnitude of the complex

bioRxiv preprint doi: https://doi.org/10.1101/660662; this version posted June 5, 2019. The copyright holder for this preprint (which was not certified by peer review) is the author/funder. All rights reserved. No reuse allowed without permission.

number Z(f) is the impedance of the neurons in a given frequency [44]. Frequencies below 0.5Hz were not analyzed and plotted because of low frequency distortions. The neuronal resonance frequency was defined at the impedance peaks; therefore, the impedance peak of a non-resonating neuron is 0.5Hz). All impedance profile analysis and calculation were done using the MATLAB 2018a software.

HCN or T-type calcium currents were isolated under voltage-clamp. The external solution for HCN current isolation contained 0.5 µM TTX, 1 mM $NiCl_2$, 1 mM $CdCl_2$, 2 mM $BaCl_2$, 10 µM DNQX and APV to block voltage-gated sodium channels, voltage-gated calcium channels, inwardly-rectifying potassium channels and excitatory synaptic current respectively. NaH_2PO_4 was omitted to prevent precipitation with cations. A standard aCSF implemented with 0.5 µM TTX (to block voltage-gated sodium channels) was used to isolated T-type calcium current. T-type calcium currents were isolated using a standard subtraction protocol [45]. Currents induced at -50mV by step voltages ranging from -90mV to 0mV were subtracted from those induced by the same step voltages depolarized from a 1 sec holding potential at -100mV to remove the inactivation of T-type calcium current. The isolated current was completely blocked by bath application of 2mM $NiCl_2$ (Supplemental Fig. 3), confirming the isolated current was T-type calcium current [46, 47].

Behavioral assays

An open field test was used to test mouse exploratory behavior and anxiety-related behavior. The experiments were all done 2 hours into the animal's dark light phase under dim red light. All mice received routine handling for a week. Three days before the experiments, mice were habituated to the training and testing room for 1 hour each day. On the first day of experiments, each mouse was placed in the open field (16 inches x 16 inches) and allowed to explore freely under dim red light for 5 minutes. Infrared beams and computer-based software

bioRxiv preprint doi: https://doi.org/10.1101/660662; this version posted June 5, 2019. The copyright holder for this preprint (which was not certified by peer review) is the author/funder. All rights reserved. No reuse allowed without permission.

Fusion were used to track mice and calculate mice activity and time spent in the center (8 inches x 8 inches) of total open field.

In novel object recognition (NOR) experiments, all mice received routine handling and three days habituation to the experimental room before the experiments. On the day before the familiarization trial, each mouse was placed in the open field in the absence of objects and allowed to explore it freely, the behaviors were recorded and analyzed further as open field test data. In the familiarization trial, each mouse was placed in the open field containing two identical 100 ml beakers in the neighboring corners for 5 minutes. Twenty-four hours later, each mouse was placed back in the same open field with two objects, one of which was the 100 ml beaker and the other one a padlock of a similar dimension, for a 5-minute testing trial. To prevent bias in objects exploration, mice were always released on the opposite side from the object for both familiarization and testing trials. For NOR and the subsequent behavior experiments, mouse behaviors in the testing trials were video-taped and analyzed by experimenters who were blind to the genotypes of the mice. Exploration of an object was defined as sniffing and touching the object with attention, whereas other behaviors like running around the object, sitting or climbing on it were not recorded as exploration [48]. Discrimination index was calculated as $(t_n - t_f)/(t_n + t_f)$. Where t_n = time exploring new object and t_f = time exploring familiar object. In the *Gbx2Cre,Shox2* KO test, 2 animals exhibited a preference for one object in the familiarization trial and therefore were not tested the next day.

The adhesive removal test was used to assess mouse paw sensorimotor response [49]. A small piece of round sticky paper tape (Tough-spots, for microtube cap ID, ~1 cm^2, Research Products International Corp. 247129Y) was applied to the plantar surface of the right hind paw

bioRxiv preprint doi: https://doi.org/10.1101/660662; this version posted June 5, 2019. The copyright holder for this preprint (which was not certified by peer review) is the author/funder. All rights reserved. No reuse allowed without permission.

of each mouse, and the mouse was placed back in its home cage and the behavior recorded. The latency to the first response to the tape was measured and analyzed.

The tail suspension test and forced swim test were applied to assess and evaluate mouse depressive-like behaviors [50]. In the tail suspension test, a 5-cm of the tip of Falcon 15 mL conical centrifuge tube was placed around the tails to prevent tail climbing, and each mouse was suspended by the tail for 5 minutes. The behavior of the mice was recorded and analyzed. The escape-related struggling time within the 5-minute experiment was measured as mobility time.

In the forced swim test, each mouse was placed in a 1000 ml beaker with ~800 ml water for 5 minutes. The behavior of the mouse was taped and analyzed by experimenters who were blinded to genotypes of the mice. Swimming and intentional movements with all four legs or body were measured as mobility time, and small movements of front or hind legs made by the animal to stay at the surface were not counted as mobility.

Fear Conditioning: Fear conditioning (habituation, training and testing) was performed and filmed in standard operant chambers (Med Associates, video fear conditioning). All behaviors were recorded, and mobility or freezing behavior was assessed online by Medical Associates Video Freeze software.

The fear conditioning protocol occurred over 4 days as follows:

Day 1: Habituation - each animal was placed in the operant chamber for 10 minutes.

Day 2: Training - each animal was placed in the chamber for a total of 8 minutes. The training trial was two mild training sessions consisting of a 30 sec auditory cue (administered at 3 and 5 minutes after placement in chamber) that co-terminated with a single 2 second 0.5 mA shock. The animal was removed from the chamber after 8 minutes.

bioRxiv preprint doi: https://doi.org/10.1101/660662; this version posted June 5, 2019. The copyright holder for this preprint (which was not certified by peer review) is the author/funder. All rights reserved. No reuse allowed without permission.

Day 3: Context Testing: Animal was placed in the chamber for 5 minutes and behaviors recorded.

Day 4: Cued testing - the chamber was modified (plastic floor and inserts to allow different shape), and different olfactory cues (vanilla) were given. The cue was administered after 3 minutes chamber exploration and freezing to the cue was assessed as described above. Animals were removed from the chamber after 6 minutes.

Statistics

Unless otherwise noted, control and KO results were compared using a Student's unpaired t-test.

Results

Shox2 is specifically expressed in the thalamic neurons in the brain of young adult mouse.

To investigate the expression of *Shox2* in postnatal mouse brain, coronal brain slices from P25 and P60 Shox2$^{LacZ/+}$ mice were stained with X-gal, in which the expression of LacZ indicated *Shox2* expression (Supplemental Fig. 4 A, B). The X-gal staining results indicated that *Shox2* is expressed throughout the dorsal thalamus including midline thalamus, anterior thalamus nuclei (ATN), ventrobasal nucleus (VB), dorsal lateral geniculate nucleus (dLGN), and medial lateral geniculate nucleus (MGN) but not in other regions of diencephalon including habenula, reticular nucleus of the thalamus and hypothalamus, or other regions of the nervous system like the cortex, subcortical regions of the forebrain, hippocampus, amygdala, cerebellum and spinal cord. To determine whether the expression pattern of *Shox2* changes during development, coronal brain slices from a P56 Shox2$^{Cre/+}$, Rosa26$^{LacZ/+}$ mouse in which LacZ is expressed in all cells that have expressed *Shox2* at any time during development were stained with X-gal (Supplemental Fig. 4C). These results showed that the expression of *Shox2* is relatively restricted to the dorsal thalamus in the adult as well as during development, with

bioRxiv preprint doi: https://doi.org/10.1101/660662; this version posted June 5, 2019. The copyright holder for this preprint (which was not certified by peer review) is the author/funder. All rights reserved. No reuse allowed without permission.

sparse expression extended to habenula and superior and inferior colliculus and nuclei within the brainstem in the developing animal. We further assessed the cell type of *Shox2*-expressing cells.

In order to determine the cell types in which *Shox2* is expressed, thalamic neurons were labeled with the neuronal nuclear protein antibody (NeuN) which is specifically expressed in mature neurons [51, 52]. *Shox2* was co-expressed in most, but not all, NeuN-positive cells throughout the dorsal thalamus from rostral to caudal (Fig. 1 A-C). Importantly, all *Shox2*-labeled cells were NeuN-positive, suggesting that *Shox2* expression is restricted to neurons. To confirm that *Shox2* was not expressed in astrocytes, the co-expression of *Shox2* and Glial Fibrillary Acidic Protein (GFAP), which labels astrocytes [53, 54] was assessed. Interestingly, GFAP was expressed at relatively low levels in the thalamus but highly expressed in the hippocampus (supplemental Fig. 5), and *Shox2* was not expressed in the GFAP-positive astrocytes throughout the thalamus (Fig. 1D-F). Together these results show that *Shox2* is expressed in neurons and not GFAP-positive astrocytes.

To determine if *Shox2* is expressed in GABAergic neurons, immunohistochemistry (IHC) with parvalbumin (PV) on coronal brain sections from $Shox2^{Cre/+}$, $Rosa26^{LacZ/+}$ mice was performed (Fig. 2). Parvalbumin (PV) is highly expressed in the interneurons of the reticular nucleus of thalamus, which borders the thalamus laterally and ventrally. PV labeling delineated the reticular nucleus that defined the border of the thalamus. The PV staining results confirmed the results shown in supplemental figure 4 that during development, *Shox2* is expressed throughout the thalamus (Fig. 2) and sparsely in the habenula (Fig. 2D) and midbrain (Fig. 2I). Importantly, *Shox2* was not expressed at any point during development in cells of the cortex (Fig. 2C), reticular nucleus of the thalamus (Fig. 2E, F), hypothalamus (Fig. 2G) or hippocampus (Fig. 2I). In addition, our results showed few PV+ cells in the thalamus as

bioRxiv preprint doi: https://doi.org/10.1101/660662; this version posted June 5, 2019. The copyright holder for this preprint (which was not certified by peer review) is the author/funder. All rights reserved. No reuse allowed without permission.

previously reported [55], and *Shox2* was not co-expressed in PV+ cells (Fig. 2G). These results suggest that *Shox2* is not expressed in parvalbumin-expressing inhibitory interneurons.

Finally, the expression and projections of *Shox2*-expressing neurons were investigated using Shox2$^{Cre/+}$; Rosa$^{tdTomato\text{-}ChR2}$ mice. These mice allow labeling of *Shox2*-expressing neurons with td-Tomato and manipulation of *Shox2*-expressing neurons with Channelrhodopsin-2. Interestingly, we found that the *Shox2*-expressing neurons projected to multiple cortical areas, including retrosplenial and somatosensory cortices with a clear delineation of the barrel fields in somatosensory cortex (Fig. 2M-O). Further strong projections from *Shox2*-expressing neurons were observed within the thalamus, particularly the VB complex, in reticular nucleus of thalamus and internal capsule (Fig. 2 M-O) projecting to somatosensory cortex. In summary, the X-gal staining and immunofluorescence results indicated that *Shox2* expression was restricted to excitatory thalamocortical neurons in the adult stage.

Lack of Shox2 affects gene expression

To study the specific role of Shox2 in regulation of gene expression in neurons of adult thalamus, RNA sequencing was performed. For this experiment, the inducible knockout (KO) of *Shox2* in *Gbx2*$^{CreERt/+}$, *Shox2*$^{-/f}$ mice were compared to littermate *Gbx2*$^{CreERt/+}$, *Shox2*$^{+/f}$ control (CR) mice. Our GFP staining results showed *Gbx2* is specifically expressed in the midline thalamus from P21 (Supplemental fig. 2), so we ran mRNA sequencing with RNA extracted from midline thalamus of the CR and KO mice. Our results showed 372 differentially expressed genes (DEG) between CR and KO mice, 212 of which are downregulated and 160 are upregulated in KO tissue (Supplemental file and Fig. 3A). Gene Ontology (GO) analysis showed *Shox2* KO affected genes in GO terms of ion channel activity, learning and locomotory behavior (Fig. 3B,C). Importantly, *Shox2* KO downregulated the expression of *Hcn2*, *Hcn4* and *Cacna1g* genes (Supplemental file and Fig. 3A). The protein products of these genes, HCN2, HCN4 and

bioRxiv preprint doi: https://doi.org/10.1101/660662; this version posted June 5, 2019. The copyright holder for this preprint (which was not certified by peer review) is the author/funder. All rights reserved. No reuse allowed without permission.

Cav3.2 mediate HCN current and T-type Ca^{2+} currents, respectively. Since these channels are significant contributors to the rhythmic firing properties of TCNs, we further pursued mRNA and protein expression of these channels.

To confirm *Shox2* regulates ion channel-related genes in the whole thalamus, another transgenic mouse line, the global KO (*Rosa26*$^{CreERt/+}$, *Shox2*$^{f/-}$ mice), in which *Shox2* was reduced in the whole thalamus was used. The RNA was extracted from KO (*Rosa26*$^{CreERt/+}$, *Shox2*$^{f/-}$ mice) and CR (*Rosa26*$^{CreERt/+}$, *Shox*$^{f/+}$) mice, and RT-qPCR was performed. The Cav3 family of Ca^{2+} channel subunits encode I_T and is highly expressed in the nuclei of the thalamus [56, 57]. We tested the levels of mRNA expression for Cav3.1 and Cav3.2, which are coded by *Cacna1g* and *Cacna1h*, respectively. Previous studies showed that Cav3.1 protein subunits are the primary T-type calcium channel proteins expressed in the thalamocortical neurons, while Cav3.2 proteins are expressed at lower levels in the thalamus and the prominent subunit in the reticular nucleus of the thalamus [58-61]. Our results showed that expression of *Cacna1h* expression was very low in the thalamus, which confirmed the specificity of our thalamic dissection (Supplemental Fig. 2C) and there was no significant difference in *Cacna1h* expression between CR and KO (Student's t-test, t9=1.02, P=0.34). With respect to the expression of *Cacna1g*, *Shox2* KO significantly decreased the mRNA expression of *Cacna1g* (Fig. 3D; Student's t-test, t9=3.85, P<0.01) in the thalamic tissue. These results confirmed the mRNA sequencing data and suggest that Cav3.1 channels that contribute to the T-type currents are down-regulated in the thalamus.

The mRNA expression of HCN channel genes in CR and KO mice was also assessed. Previous studies reported that mouse brains express very low levels of *Hcn3* [62], and our RNA-seq data showed no significant change in *Hcn3* or expression in the KO mice, therefore, *Hcn3* expression was not further investigated. The expression levels of mRNAs for *Hcn1*, *Hcn2*, and

bioRxiv preprint doi: https://doi.org/10.1101/660662; this version posted June 5, 2019. The copyright holder for this preprint (which was not certified by peer review) is the author/funder. All rights reserved. No reuse allowed without permission.

Hcn4 were investigated. *Hcn2* mRNA was the most highly expressed HCN channel gene in the thalamus tissue. *Hcn4* also had prominent expression, while the level of expression of *Hcn1* was only about 5% of *Hcn2* expression. This result is consistent with previous research indicating HCN2 and 4 channels are the most highly expressed HCN channels in the thalamus, and these results along with our sequencing results, provide relative expression data of HCN mRNA expression in mouse thalamus [62]. *Hcn1* mRNA expression levels were not significantly affected by *Shox2* KO in comparison to CR mice (t_9=1.85, P=0.10). *Hcn2* and *Hcn4* mRNA were significantly reduced in the *Shox2* KO thalamus compared to CR mice (Fig. 3E, F, *Hcn2*: t_9=3.92, P<0.01 and *Hcn4*: t_9=4.02, P<0.01). This result also confirmed the RNA-seq results that showed that *Hcn1* mRNA was not significantly affected in mouse thalamus. Together, these results show that *Shox2* KO significantly affects expression of mRNAs for HCN and Ca^{2+} channels. We further investigated if the proteins for these channels were also affected in the KO mice.

Western blot experiments on whole thalamus extract were performed to test the protein levels of the Cav3.1, HCN2 and HCN4 channels. The expression levels of HCN2 and HCN4 proteins were significantly decreased in the thalami of KO animals, and there was a trend toward decreased expression of Cav3.1 protein compared to CR mice (Fig. 3G,H,I; Cav3.1: t_{14}=1.86, P=0.08; HCN2: t_{16}=2.30, P=0.04; HCN4: t_{14}=2.37, P=0.03). The protein measurements in these Western blot staining results are consistent with sequencing and RT-qPCR results, and confirmed that HCN2, HCN4 and Cav3.1 protein expression is modulated by Shox2 in the adult thalamus. While the change in expression of these channels is relatively small, it's important to note that these data are taken from the entire thalamus, including neurons and glial cells that do not express *Shox2*. The consistency of the sequencing, mRNA and protein expression is solid evidence that *Shox2* affects expression of these ion channel genes.

bioRxiv preprint doi: https://doi.org/10.1101/660662; this version posted June 5, 2019. The copyright holder for this preprint (which was not certified by peer review) is the author/funder. All rights reserved. No reuse allowed without permission.

Since the expression levels of the channel proteins that underlie currents important for the bursting properties of the thalamic neurons are regulated by *Shox2* expression, we assessed the firing and intrinsic properties of thalamic neurons in *Shox2* KO and CR mice. To best identify a single thalamic nucleus and a homogenous neuron group, the anterior paraventricular thalamus (PVA), the most rostral and dorsal midline nucleus, was chosen as the target region for recording. First, cell-attached voltage-clamp recordings were performed to record the spontaneous action potential currents of PVA neurons without rupturing the cell membrane. Our results indicated that a smaller percentage of cells fired spontaneous action potentials (active neurons) in KO mice compared to those in CR mice (Fig. 4A, CR: 36% vs KO: 14%; $\chi 2$ test, $\chi 2=3.84$, $P=0.05$). We also conducted whole-cell current clamp recordings and tested spontaneous action potential firing at resting membrane potential. Slices from KO mice consistently showed a significantly lower percentage of spontaneously active neurons (Fig.4B, CR: 47% vs KO: 18%; $\chi 2$ test, $\chi 2=7.60$, $P<0.01$). The decreased cell excitability in PVA neurons from the KO mice was not due to significant differences in resting membrane potential between CR and KO cells (CR: -55.5±1.7 (n=35) and KO: -54.5±1.7 (n=35), p = 0.9); however, input resistance was significantly different between cells recorded from KO and CR mice (CR: 993.4±52.86 (n=30) KO: 850.3±40.73 (n=29); p = 0.04). These results suggest that reduced Shox2 expression affects the firing properties of TCNs.

To investigate the voltage response to small depolarizations, we recorded in current clamp mode and injected 10pA and 20pA currents to evoke action potentials from resting potential and -70mV. Action potential frequency in neurons recorded from *Shox2* KO slices was significantly decreased compared to that in neurons from CR slices both at resting potentials (two-way repeat measures ANOVA: main effect of current injection, $F_{1,44}=19.9$, $P<0.001$; main effect of genotype, $F_{1,44}=4.90$, $P<0.001$; interaction, $F_{1,44}=7.71$, $P<0.01$; post-

bioRxiv preprint doi: https://doi.org/10.1101/660662; this version posted June 5, 2019. The copyright holder for this preprint (which was not certified by peer review) is the author/funder. All rights reserved. No reuse allowed without permission.

hoc Bonferroni's test: CR vs KO at 20pA current injection, P<0.001) and -70mV (Fig. 4C, Two way repeated measures ANOVA: significant main effect of genotypes (CR vs KO, $F_{(1, 60)} = 4.2$, P=0.04) and current injection (10pA vs 20pA, $F_{(1, 60)} = 36.60$, P<0.001) in the number of evoked spikes in 1s depolarization from -70mV. These results are consistent with the spontaneous firing results that suggest that reduced *Shox2* affects TCN firing properties.

In order to assess a role for the HCN and Ca^{2+} currents, rebound bursting was induced by injection of negative currents at -70mV [63]. The latency to the peak of rebounded calcium spikes was significantly longer in neurons from *Shox2* KO slices than that in neurons from CR slices (Fig. 4D; t_{21}=2.29, P=0.03). Neurons from *Shox2* KO slices had a slower decay phase of the spike rebound, and therefore, a longer spike duration as indicated by a larger area under the voltage trace (Fig. 4D; t_{24}=2.11, P=0.05). These results suggest that *Shox2* expression affects Ca^{2+} currents and may also affect currents important for repolarization of the depolarizations, primarily K^+ currents.

To further determine the effects of Shox2 expression on thalamus neuron firing properties, the response to a slow ramp of depolarizing current (50pA in 60s, 0.83pA/s) in PVA neurons was determined. The results showed that the ramp currents induced low threshold bursts followed by a tonic or sparse spike train (Fig. 5A, B). The thresholds of the first action potentials of KO neurons were significantly depolarized compared to those of CR neurons (Fig. 5C), and the duration to the first action potential was significantly longer in the neurons from the *Shox2* KO mice (Fig. 5D). These results suggest delayed and higher firing threshold in *Shox2* KO neurons, properties that may be affected by T-type and K^+ currents.

Previous frequency domain research demonstrated that thalamocortical neurons resonate in the 2-4 Hz range near membrane potential [64, 65]. This preferred membrane resonant behavior contributes to frequency selectivity and is correlated to burst firing mode

bioRxiv preprint doi: https://doi.org/10.1101/660662; this version posted June 5, 2019. The copyright holder for this preprint (which was not certified by peer review) is the author/funder. All rights reserved. No reuse allowed without permission.

and membrane potential oscillations [44, 66]. Furthermore, previous studies indicate that HCN channels mediate the resonance properties of neurons at hyperpolarized potentials [67, 68], therefore, we investigated the resonance properties of the thalamocortical neurons at resting membrane potential in *Shox2* KO animals. A ZAP current stimulus was applied to PVA neurons and the voltage response was recorded to determine the resonance frequency (Fig.5E,F). We found that most neurons from CR mice had maximum peaks of impedance at a frequency ranging between 1Hz and 3Hz (Fig. 5E,F), while neurons from *Shox2* KO mice had maximum impedance at a lower frequency (<0.5Hz) without apparent peaks (Fig. 5E,F). The summary bar graph shows that *Shox2* KO neurons have a reduced resonance frequency compared to CR neurons (Fig. 5G). This effect of Shox2 expression on the resonance frequency likely contributes to an impaired ability to transmit sensory information to the cortex and suggests that burst firing and oscillatory modes of thalamocortical function are dysregulated in the *Shox2* KO mice.

Shox2 is critical for HCN current and T-type calcium current in the thalamus.

The sequencing and Rt-qPCR results indicating reduced expression levels of channels and the changes in both cell excitability and intrinsic properties of PVA neurons in *Shox2* KO mice suggest that *Shox2* modulates intrinsic currents, especially HCN and T-type currents which contribute to cell excitability, rebound after-hyperpolarization and resonance. Therefore, we hypothesized that *Shox2* KO impaired pacemaker-related T-type calcium current and HCN currents in PVA neurons.

First, we determined the physiological properties of T-type calcium currents in CR and *Shox2* KO. We isolated T-type calcium current in the PVA neurons (Fig. 6) with a typical subtraction protocol as described in the methods [45]. Although the activation voltage range of T-type currents in neurons from both CR and KO mice fell between -70mV to -10mV with a

bioRxiv preprint doi: https://doi.org/10.1101/660662; this version posted June 5, 2019. The copyright holder for this preprint (which was not certified by peer review) is the author/funder. All rights reserved. No reuse allowed without permission.

peak at -50mV (Fig. 6A, B), the activated current density was significantly decreased in the PVA neurons from KO mice (Fig. 6B, two-way repeated measures ANOVA, main effect of genotype: $F_{1,20}$ = 8.70, P<0.01; main effect of voltage: $F_{9,180}$ =63.98, P<0.001; interaction: $F_{9,180}$ =6.38, P<0.001). A post-hoc Bonferroni's multiple comparisons test revealed that the current density elicited at -60 mV (-7 ± 2.7 pA) and -50 mV (-12.3 ± 1.4 pA) in CR neurons was significantly larger than that in KO neurons (-60 mV: -0.73 ± 0.5 pA and -50 mV: -8.1±1 pA; Fig. 6B, P<0.001). Two-way repeated measures ANOVA of normalized T-type calcium activation curve revealed a significant interaction between genotype and voltage ($F_{9,180}$ =3.27, P<0.01) and post-hoc Bonferroni's test showed that the normalized T-type calcium current (I/Imax) was significantly decreased at -60mV in KO mice compared CR mice (Fig. 6C, CR: 0.36 vs KO: 0.08, P<0.01). This suggests the activation of the T-type calcium current is shifted toward more depolarized membrane potentials in the neurons from the KO mice and is consistent with the delayed threshold of low-threshold-spike in KO neurons in Figure 5. In addition, the time to peak of the T-type current measured at -50 mV in *Shox2* KO neurons was significantly slower compared to CR neurons (Fig. 6D; t_{20} =2.57, P=0.02). The slower kinetic properties of T-type calcium current occurred during the activation (P=0.08) but not inactivation phase (P=0.97).

The inactivation properties of the T-type calcium currents were determined by eliciting inactivation of the T-type calcium currents at -50mV after a 1-second hyperpolarizing potential ranging from -90mV to -40mV (Supplementary Fig. 3E). This curve confirmed that the current density was decreased in neurons from KO mice compared to neurons from CR mice (two-way ANOVA, the main effect of genotypes, $F_{(1,\ 21)}$ = 8.41, P<0.01). However, the normalized inactivation curves of T-type calcium currents from neurons from CR mice and neurons from KO mice were not significantly different (Supplemental Fig. 3), suggesting that the inactivation kinetics of the T-type currents were not different between CR and KO mice.

bioRxiv preprint doi: https://doi.org/10.1101/660662; this version posted June 5, 2019. The copyright holder for this preprint (which was not certified by peer review) is the author/funder. All rights reserved. No reuse allowed without permission.

Kinetics analysis revealed that the T-type current in neurons from *Shox2* KO mice have a longer time to peak and slower inactivation time constant compared to neurons from CR mice. The T-type calcium current window, defined by the area under both the activation and inactivation curves, which contributes to the large-amplitude and long-lasting depolarization, or UP state, of the slow (<1 Hz) sleep oscillation in thalamic neurons [69-73], was greater in neurons from CR mice compared to neurons from KO mice (Fig. 6E). This is particularly striking in the potential range between -60mV and -70mV (Fig. 6E,F) and suggests that the effect of *Shox2* expression on the T-type current is particularly important near resting membrane potential and may contribute to slow oscillations.

Second, since HCN currents also play a role in the burst firing properties of thalamocortical neurons [74, 75], and *Shox2* affects expression of both *Hcn2* and *Hcn4* mRNAs and proteins, we investigated the effect of Shox2 KO on HCN current by sequential hyperpolarizations in voltage-clamp mode. The amplitude of HCN current was measured as the difference between the end current of one-second hyperpolarization and the beginning instantaneous current at -150mV hyperpolarization (Fig. 6G). The HCN current densities in neurons from *Shox2* KO mice were significantly decreased compared to neurons from CR mice (Fig. 6H).

Shox2 KO induced thalamus-related behavioral deficits in adult mouse.

The thalamus plays a critical role in sensory and motor information relay and processing, sleep and arousal, learning and memory, as well as other cognitive functions. The electrophysiological results indicated that *Shox2* KO impaired thalamic burst-related currents and intrinsic spiking properties. We hypothesized that *Shox2* is critical for proper cognitive and somatosensory behavioral functions in adult mice. To study the specific contribution of *Shox2* expression in the thalamus to behaviors, including anxiety, depression, somatosensory

bioRxiv preprint doi: https://doi.org/10.1101/660662; this version posted June 5, 2019. The copyright holder for this preprint (which was not certified by peer review) is the author/funder. All rights reserved. No reuse allowed without permission.

information processing as well as learning and memory, two inducible KO mouse strategies were employed. For the behavioral studies, we used the *Rosa26*$^{CreERt/+}$, *Shox2*$^{-/f}$ mice line which is a tamoxifen-inducible global *Shox2* KO, and the *Gbx2*$^{CreERt/+}$; *Shox2* $^{-/f}$ mice line which is also tamoxifen-inducible but restricts the KO of Shox2 specifically in the midline of the thalamus [76, 77] and supplemental Fig. 2.

The total distance travelled in an open field test was measured to investigate the overall activity and general anxiety levels. Distance travelled in the open field in the global *Shox2* KO mice was not statistically significant compared to CR mice (Fig. 7A, t_{26}=1.48; p = 0.15). Interestingly, the global KO mice spent a significantly higher percentage of time in the center of the open field compared to CR mice (Fig. 7B, t_{26}=2.2; P=0.04), which is indicative of lower levels of anxiety in the KO mice [78].

Because the open field test results suggested that global *Shox2* KO mice exhibited lower anxiety, we investigated depressive-like behaviors using the tail suspension test and the forced swim test in another cohort of animals [79]. In these tests, the time during which the animals were actively struggling was measured as mobility time. We observed no significant difference in mobility time between control and global KO mice in either test (Forced swim test, t_{20} =0.39, P=0.70; Tail suspension, t_{20}=0.85, P=0.40; Supplemental Fig. 5A,B), suggesting *Shox2* KO did not affect depressive-like behaviors.

To test the performance of the mice in general somatosensory function, the paw sensation test was performed. Sticky tape was applied to the plantar surface of the right hind paw of each mouse, and the latency to the mouse's first reaction to the tape was measured [49]. The latency of KO mice to react to the tape was significantly longer than that of CR mice (Fig. 7C; t_{26}=2.38, P=0.03). The results suggested that *Shox2* KO induced somatosensory deficits in adult mice.

bioRxiv preprint doi: https://doi.org/10.1101/660662; this version posted June 5, 2019. The copyright holder for this preprint (which was not certified by peer review) is the author/funder. All rights reserved. No reuse allowed without permission.

Given that anterior and medial thalamus are critical for learning and memory processes [80-83], we tested a subset of the global *Shox2* KO mice in a novel object recognition test which assesses learning and memory functions [84, 85]. The test consisted of a familiarization trial and a test trial. During the familiarization trial, we measured the time mice spent exploring 2 identical novel objects (see methods) in the open field environment. Animals of both genotypes explored the 2 objects for similar amounts of time (Fig. 7E, Student's t-test, t_{1p}=1.7, P=0.1). Twenty-four hours later, in the memory test trial, the experiment was repeated but one of the beakers was replaced with a new object (Fig. 7D). The percentage of time global *Shox2* KO mice spent around the novel object was significantly decreased compared to that of CR mice in the testing trial (Fig. 7F; t_{19} =2.1, P=0.05). These results suggest an impairment of learning and memory ability of global *Shox2* KO mice.

In order to determine whether the impairment in the object recognition test was mediated by sensory or memory function, we also performed similar behavioral analysis in the Gbx2^{CreERt}; *Shox2* KO mice (Fig. 7 G-K), where *Shox2* is reduced specifically in the midline thalamus. The open field test was conducted to investigate the overall activity and general anxiety level of CR and GBX2^{CreERt}; Shox$^{fl/-}$ KO mice. The total distance travelled by *Shox2* KO mice was not significantly different compared to CR mice (Fig. 7G, t_{21}=0.92; p = 0.37). In addition, unlike the global KO mice, the time spent in the center of the open field of Gbx2^{CreERt}; Shox$^{fl/-}$ KO compared to CR mice was not significantly different (Figure 7H, t_{21}=0.50; p = 0.62). We also tested the performance of these mice in general somatosensory function, with the paw sensation test. The latency to react to the tape of KO mice was not significantly different compared to CR mice (Fig. 7C; t_{20}=0.4626, P=0.65). The tape fell off the foot of one KO mouse, therefore results from that animal were not used. The results suggested that *Shox2* KO in the midline thalamus did not affect somatosensory function.

bioRxiv preprint doi: https://doi.org/10.1101/660662; this version posted June 5, 2019. The copyright holder for this preprint (which was not certified by peer review) is the author/funder. All rights reserved. No reuse allowed without permission.

We also tested the Gbx2^{CreERt}; Shox$^{fl/-}$ mice in the novel object recognition test as described above. Animals of both genotypes explored the 2 objects for similar amounts of time in the familiarization trial (Fig. 7J, Student's t-test, t_{18}=1.64; P=0.11). Twenty-four hours later, in the memory test trial, the experiment was repeated but one of the beakers was replaced with a new object (Fig. 7D). The percentage of time Gbx2^{CreERt}; Shox$^{fl/-}$ mice spent around the novel object was significantly decreased compared to that of CR mice in the testing trial (Fig. 7F; t_{18}=2.28; P=0.04). These results suggest an impairment of memory formation in the Shox2 KO mice in the midline thalamus, consistent with studies that show the midline thalamus is important for cognitive function.

Since the anterior and midline thalamus have also been implicated in fear memory formation [86], cued and contextual fear memory was assessed. Neither contextual (t_{21}=0.52; p = 0.61 nor cued fear memory (t_{20}=0.1.4; p = 0.17, freezing in one mouse was excluded as an outlier) was affected in the Gbx2^{CreERt}; Shox$^{fl/-}$ KO mice (Supplemental Fig. 5C,D). This result is supported by our observations made in td-Tomato animals that show sparse direct inputs to the hippocampus and the amygdala (Fig. 2M-O). Together, these results suggest that the groups of neurons expressing *Shox2* in midline thalamus support recognition memory but are not implicated in fear memory formation or somatosensory information processing.

Discussion

This study demonstrates the importance of transcriptional activity of the homeobox protein transcription factor, Shox2, in regulation of firing properties and function of thalamocortical neurons in adult thalamus. This assertion is supported by our investigations at genetic, electrophysiological and behavioral levels. Genetic analysis via RNA-sequencing and Gene Ontology (GO) analysis revealed that Shox2 modulates expression of genes that

bioRxiv preprint doi: https://doi.org/10.1101/660662; this version posted June 5, 2019. The copyright holder for this preprint (which was not certified by peer review) is the author/funder. All rights reserved. No reuse allowed without permission.

encode for proteins directly associated with firing properties of TCNs, specifically voltage-gated ion channels. Further investigation using quantitative PCR and Western blotting showed that the mRNAs and proteins for several of these ion channels, namely HCN2, HCN4 and Cav3.1, are all down-regulated in the thalamus of the *Shox2* KO. Electrophysiological analysis revealed that *Shox2*-regulation of these channels contributes to the intrinsic firing properties in these neurons mediated by the corresponding HCN current and T-type Ca^{2+} current. Finally, behavioral investigation revealed that global *Shox2* KO mice were impaired in an object memory and somatosensory function test, suggesting that *Shox2* is important to maintain normal function of thalamocortical neurons. In order to discern the somatosensory deficit from the object memory function, we further investigated mice with specific KO of Shox2 in the midline thalamus KO (*Gbx2*^{CreErt}-*Shox2*), which maintained Shox2 expression in the lateral thalamus, specifically the VB complex important for somatosensory processing. These mice were impaired in the object recognition task and not sensorimotor functions, suggesting that Shox2 expression in the TCNs of the midline thalamus is important for cognitive function. These studies are consistent with previous results that show lesions to the anterior thalamic nuclei can disrupt object recognition memory in animal models [80, 82, 83, 87].

Previous clinical studies demonstrate that proper thalamic function is critical for memory formation and consolidation. In humans, damage to the thalamic nuclei, especially medial and anterior nuclei, causes severe memory deficits known as diencephalic amnesia [12-17]. While the neural circuitry of the effects of Shox2 expression on recognition memory are unclear, perhaps these effects occur via effects on TCN connections to retrosplenial cortex as suggested by the anatomical connectivity indicated in our study (Fig. 2 M-O). The retrosplenial cortex has been linked to temporal order of recognition, also known as 'what and when' associations [88]. Future

bioRxiv preprint doi: https://doi.org/10.1101/660662; this version posted June 5, 2019. The copyright holder for this preprint (which was not certified by peer review) is the author/funder. All rights reserved. No reuse allowed without permission.

studies are necessary to determine the specific projections and functions of the firing properties of the TCNs involved in these functions.

The functions of the burst and tonic firing properties of thalamocortical neurons are still under investigation. Tonic spike firing mode is thought to contribute to reliable information transfer during perceptive states that conveys sensory information to cortex [89, 90]. Burst firing mode may allow lack of responsiveness to sensory input during sleep and unconsciousness such as during an absence seizure [91-94]. On the other hand, recent evidence suggests that thalamic bursts can also occur during awake states and convey a high degree of information about sensory stimuli to serve as a 'wake-up call' for cognitive attention [95-100]. Computational studies suggest that the bursting behavior occurs in response to low-frequency stable inputs, while single spikes occur in response to higher frequency more dynamic input [101, 102]. Disruptions in the transitions of firing patterns through effects on intrinsic currents in TCNs would disrupt normal thalamic function and its contribution to information processing. Our present studies from the thalamus, together with studies of Shox2 function from the heart [103, 104] and excitatory interneurons in spinal cord [34, 36], suggest that *Shox2* is important for maintenance of repetitive, low-frequency burst firing properties partially through regulation of channels that support I_h and I_t function.

Several lines of evidence indicate that these studies of the role of *Shox2* in pacemaker function in mice are also applicable to humans. *Shox2* is a super-conserved gene with 99% amino acid identity between human SHOX2 and mouse *Shox2.* A recent study found that two missense mutations within the human *SHOX2* gene are associated with early-onset atrial fibrillation, likely caused by a defect in pacemaker activity [105, 106]. In addition, while mice do not express the *Shox* gene, human *SHOX* and *SHOX2* have 79% similar amino acid identity, and the same DNA-binding domains and putative phosphorylation sites. The functional

bioRxiv preprint doi: https://doi.org/10.1101/660662; this version posted June 5, 2019. The copyright holder for this preprint (which was not certified by peer review) is the author/funder. All rights reserved. No reuse allowed without permission.

redundancy in the regulation of heart pacemaker cells' differentiation between human *SHOX* and mouse *Shox2* has been demonstrated in mouse models [104, 107]. Therefore, investigation of *Shox2* function in mouse can extend to evaluate the role of human *SHOX* and *SHOX2* in humans. Turner syndrome (TS) is one of the most common sex chromosome abnormalities [108, 109] and results from the complete or partial loss of the X chromosome. Most individuals with TS have short stature, which is associated with the loss of the SHOX gene [110-112]. These individuals are at increased risk for neurodevelopmental issues, including learning disabilities, visuo-spatial, social and executive function impairments [113] and epilepsy [114-118]. Interestingly, the smallest chromosomal deletion associated with the neurocognitive phenotype included *SHOX* [119], suggesting that loss of SHOX may play a role in cognitive impairments in humans. While the mechanisms of the neurodevelopmental issues in these patients is unclear, our current study indicates that altering expression of SHOX- or SHOX2-related genes may contribute to thalamic dysfunctions and some of these neurodevelopmental impairments.

Further studies are necessary to determine the specific contribution of Shox2-expressing neurons to thalamocortical circuitry, and the role Shox2 may play beyond regulation of firing properties. In addition, future studies will investigate whether *Shox2* plays a critical role during thalamus development and differentiation, the contribution of these *Shox2*-regulated currents to overall thalamocortical neuron function, and the mechanisms by which *Shox2* regulates their expression.

Figure Legends

Figure 1. *Shox2* is expressed in NeuN+ neurons in the thalamus and not in GFAP+ astrocytes. Coronal brain sections through the thalamus of *Shox2*$^{Cre/+}$, Rosa26LacZ mice were co-stained with NeuN (green) and β-gal (red). Three typical thalamic regions are shown, including anterior paraventricular thalamus (PVA) (**A**), dorsal lateral geniculate nucleus (dLGN) (**B**), and ventrobasal nucleus (VB) (**C**). Slices were co-stained for NeuN and the reporter for *Shox2*, β-gal. *Shox2* is expressed in NeuN+ neurons (red, merged). Right panels are magnifications of

bioRxiv preprint doi: https://doi.org/10.1101/660662; this version posted June 5, 2019. The copyright holder for this preprint (which was not certified by peer review) is the author/funder. All rights reserved. No reuse allowed without permission.

the boxed regions respectively, showing cells that co-express *Shox2* and NeuN. **D-F** show the co-expression of astrocyte marker GFAP (green) and β-gal (red), in three thalamic regions: PVA (**D**), dLGN (**E**) and VB (**F**). Right panels are magnifications of the boxed regions. The arrowheads show the GFAP+ glia, and the white arrows show *Shox2*-expressing cells as indicated by β-gal. No cells co-expressed GFAP and *Shox2*. RT: reticular thalamus. AV: anteroventral nucleus of the thalamus; AD: anterodorsal nucleus of the thalamus. HP: hippocampus

Figure 2. *Shox2* is expressed in glutamatergic thalamocortical neurons but not parvalbumin+ interneurons. Coronal sections through the thalamus were co-stained with parvalbumin (green, **A, B**) and β-gal (red, **A, C**). Boxes in Figure **A** are magnified in **D.** (habenula), **E.** Ventrobasal (VB) and reticular nucleus (RT), and **F.** dorsal lateral geniculate nucleus (dLGN). **G**. Panels G-I show *Shox2* expression in coronal slices of rostral to caudal thalamus (**G**: Paraventricular nucleus of the thalamus (PVA) relative to Bregma, approx. -1.1; **H**: lateral geniculate nucleus (LGN) -2.0; **I**: Medial geniculate nucleus (MGN) –2.9). **M-O:** Coronal sections from rostral (M) to caudal (O) from the Ai27D-*Shox2Cre* in which the presence of tdTomato indicates *Shox2*-expressing neurons. *Shox2* is expressed in neurons throughout the thalamus and projections to the cortex, strongly targeting layer IV barrel cortex (white arrows) and layer VI.

Figure 3. Shox2 expression affects gene expression and ion channel protein levels. RNA-sequencing and analysis were performed as described in methods. **A**. Heatmap, made by pheatmap, saturated at 1, displays 367 DEGs (adjust p value <0.1) in the midline thalamus between control (CR) and *Gbx2*^{CreErt,} *Shox2* KO mice. **B.** Ingenuity Pathway Analysis revealed *Shox2* KO-induced DEGs are highly involved in thalamus-related neurological diseases. **C**. Gene ontology (GO) enrichment analysis of DEGs. All terms with an FDR (analyzed by DAVID functional annotation tool) less than 0.1 are listed. **D-F.** RT-qPCR results show that *Shox2* KO significantly reduced mRNA level of *Cacna1g*. **(D),** *Hcn2* **(E)** and *Hcn4* **(F)**. **G-I.** *Shox2* KO decreased the protein expression levels of $Ca_v3.1$ (**G**, ~120kD), HCN2 (**H**, ~150kD), and HCN4 (**I**, >250kD) (**, p < 0.01; *, p<0.05, #, p<0.1). The bands around ~55-60kD are recognized by the β-tubulin antibody.

Figure 4. Shox2 KO decreases the ratio of cells with spontaneous action potentials in the anterior paraventricular thalamus (PVA). A. Example traces of attached-cell recordings of active cells showing spontaneous action potentials (left) and inactive cells with no action potentials (right). Bar graph representing the ratio of active and inactive cells recorded in PVA from KO and CR mice. This ratio is significantly smaller in KO than in CR mice (**, p<0.01). **B.** Upper: Example trace of action potential induced by a 1sec, 10 pA and 20pA current injection steps while holding membrane potential at -70mV. Lower: Scatter plot graph showing that the number of spikes induced by 10pA and 20pA current injection at -70mV was reduced in the KO mice (gray) relative to control mice (black). **C**. Upper: Example traces of rebound spikes triggered by injection of negative current steps (-50 pA, -100 pA and -150pA) from a holding potential of -70mV. Lower – left: The latency to the peak of calcium spike after current injection is significantly longer in *Shox2* KO neurons than in control neurons. Lower – right: The areas under voltage traces (between spike traces and -70mV) indicating plateau depolarizations are significantly larger in *Shox2* KO neurons (arrow) than neurons from control mice (*, p < 0.05, **; p < 0.01, ***; p <0.001).

bioRxiv preprint doi: https://doi.org/10.1101/660662; this version posted June 5, 2019. The copyright holder for this preprint (which was not certified by peer review) is the author/funder. All rights reserved. No reuse allowed without permission.

Figure 5. Shox2 is important for action potential firing characteristics. A. Example traces of firing patterns triggered by the injection of ramp current in cells recorded from CR – left, black) and B. KO mice (right, blue). **C**. Quantification of the burst threshold potential in CR and KO cells. The threshold is significantly more depolarized in KO cells. **D**. Latency to action potential firing from CR and KO mice in response to ramp current injection. The latency is significantly longer in KO cells. **E.** Variable-frequency oscillatory waveforms showing the voltage response to the sine wave input current (20-0 Hz over 20 seconds) and corresponding power spectra. **F.** The resonance frequency measured in CR (left) and KO (right) mice. **G.** Quantification shows that the preferred intrinsic frequency of recorded neurons was around 3 Hz in CR mice, but KO mice lacked measurable resonance frequency (*, $p < 0.05$, **, $p < 0.01$).

Figure 6. Properties of T-type calcium and HCN currents in PVA neurons of CR and *Shox2* KO mice. A-D. The T-type calcium currents were isolated using voltage-clamp recordings according to methods. **A.** An example of T-type calcium currents recorded from PVA neurons of CR and *Shox2* KO mice. T-type calcium currents in *Shox2* KO mice are smaller in amplitude and slower than in CR mice. **B.** The current density curve of T-type calcium current activation. T-type calcium current density is smaller in PVA neurons of KO mice compared to CR mice (***, $p < 0.001$). **C.** The normalized activation curves indicate that T-type calcium (I/I_{max}) is larger at -60mV in CR mice than that in KO mice (***, $p < 0.001$). **D.** Summary plot showing the time to peak (*, $p < 0.05$), activation and inactivation tau of the T-type current in TCNs from CR and KO mice. **E.** Inactivation and activation curves of T-type currents. **F**. Membrane potential range magnified to show T-type Ca^{2+} currents in -70 to -50 mV membrane potential window range. **G**. Shox2 KO decreased HCN current in anterior PVT of neurons. An example of HCN current elicited by hyperpolarizing cell membrane from -50mV to -100mV and -150mV. HCN current is defined as the current difference between the current at the end of 1s hyperpolarization and the current peak at the beginning of hyperpolarization as shown in the figure. B. **H**. Scatter plot showing that *Shox2* KO decreased HCN current density in anterior PVT of neurons ($P<0.01$).

Figure 7. Shox2 inducible KO caused comprehensive thalamus-related behavior deficits. A. Results from open field analysis. The total distances travelled by $Rosa^{CreErt}$, *Shox2* KO and CR mice in 5-minute open field test were similar. **B**. $Ros^{CreErt,}$ *Shox2* KO mice spent a higher percentage of time in the center of open field than CR mice (*, $P<0.05$). **C.** Mice with a ~1 cm^2 sticky tape on the left hind paw were placed in home cage and the latency for the mice to first react to the tape was measured. *Shox2* KO mice had a longer latency to first react to the tapes than CR mice ($P<0.01$). **D.** Schematic diagram showing experimental design of novel object recognition (see methods). **E-F.** The results of discrimination index showed that *Shox2* KO impaired mice ability in recognizing novel object in testing trial (*, $P=0.02$), while there was no object preference difference between CR and KO mice in familiarization trial ($P =0.33$). **G.** The total distance travelled by $Gbx2^{CreErt}$, *Shox2* KO mice in 5-minute open field test was significantly decreased compared to that by CR mice. **H.** $Gbx2^{CreErt,}$ *Shox2* KO mice spent a similar percentage of time in the center of compared to CR mice. **I.** $Gbx2^{CreErt,}$ *Shox2* KO mice were not significantly different from CR in the sticky tape test. **J-K**. Object recognition task in $Gbx2^{CreErt,}$ *Shox2* KO mice. The results of discrimination index showed that $Gbx2^{CreErt,}$ *Shox2* KO

bioRxiv preprint doi: https://doi.org/10.1101/660662; this version posted June 5, 2019. The copyright holder for this preprint (which was not certified by peer review) is the author/funder. All rights reserved. No reuse allowed without permission.

impaired mice ability in recognizing novel object in testing trial ($p < 0.05$) (K), while there was no object preference different between CR and KO mice in familiarization trial (J).

Supplemental Figures

Supplemental Figure 1. Schematic diagrams of breeding schemes used to produce Rosa26$^{CreERt/CreERt}$, Shox2$^{f/-}$ and *Gbx2*$^{CreErt/CreErt}$, *Shox*$^{f/-}$ mice.

Supplemental Figure 2. Characterization of *Gbx2* expression and *Gbx2*-induced *Shox2* KO in thalamus. A. GFP staining (red color) represented the expression pattern of *Gbx2* in P25 mouse brain, showing *Gbx2* only expressed in the midline of the thalamus (arrow shows PVT in midline thalamus) but not lateral thalamus. Blue: DAPI. **B**. qPCR results demonstrating significant knockdown of *Shox2* mRNA in midline thalamus of *Gbx2*$^{CreErt/CreErt}$, *Shox*$^{f/-}$ mice compared to CR mice (t_6=3.9, p = 0.008), but no effect on *Shox2* mRNA expression in the lateral thalamus compared to CR animals (**, p<0.01).

Supplemental Figure 3. Isolation of T-type Ca^{2+} current: **A.** The membrane potential was hyperpolarized to -100mV for 1s from holding potential -50mV to remove inactivation of the T-type calcium current. **B.** T-type calcium currents were elicited by stepping from -100mV to a series of incremental depolarizations ranging from -90mV to 0mV. **B.** The same series of step voltages was applied to the same neurons without hyperpolarization to -100mV, instead, the membrane potential was held at -50mV in that time range. **C.** The T-type calcium currents were isolated by subtracting currents evoked in B from currents evoked in A. **D**. The isolated current was blocked by 2mM $NiCl_2$, confirming the isolated current is T-type calcium current. **E**. The T-type calcium currents were elicited at -50mV after recovery from 1s pre-holding step voltage ranging from -90mV to -40mV. The elicited T-type calcium current is confirmed by application of 2mM $NiCl_2$ to block it. **F.** The curve of T-type calcium current inactivation current density at different pre-holding voltage from CR neurons and KO neurons. Two-way repeated measures ANOVA indicated significant main effect of genotypes (CR vs KO, $F_{(1,21)}$ = 8.41, P<0.01) and voltage ($F_{(5,105)}$ =218.7, P<0.001) and significant interaction (F(5,105)=8.58, P<0.001). D. The normalized inactivation current curves of CR and KO neurons are overlapped with each other.

Supplemental Figure 4. Shox2 expression is restricted to thalamus in adult and diencephalon throughout development. Brain sections demonstrating X-gal staining (or Shox2 expression) results from PND25 **(A1-A8)** and PND56 Shox2$^{LacZ/+}$ **(B1-B4)** and PND56 male Shox2$^{cre/+}$, Rosa26$^{LacZ/+}$ mouse **(C1-C4).** X-gal staining was observed in anterior thalamus nuclei (ATN), anterior paraventricular nucleus (PVA), ventrobasal thalamus (VB), dorsal lateral geniculate nucleus (dLGN) and medial geniculate nucleus (MGN) but was not observed in the cortex (CX), striatum (STR), hippocampus (HP), amygdala (Ag) or hypothalamus (HT). During development, *Shox2* did express in in habenula (HB), and some areas of the midbrain including superior colliculus (SC) and inferior colliculus (IC), but this expression is reduced in adults. Scale bar: 2 mm.

Supplemental Figure 5. Strong GFAP immunoreactivity in the hippocampus, but a lack of

bioRxiv preprint doi: https://doi.org/10.1101/660662; this version posted June 5, 2019. The copyright holder for this preprint (which was not certified by peer review) is the author/funder. All rights reserved. No reuse allowed without permission.

GFAP+ staining in the thalamus. Coronal brain section showing strong GFAP+ staining in the hippocampus, but a dearth of GFAP staining in the thalamus.

Supplemental Figure 6. Behavioral analysis of Shox2 KO mice. Mobility results measured from CR and *RosaCre;Shox2* KO mice. Forced swim test **(A)** and tail suspension test **(B)**. No significant differences in struggling time between CR and KO mice were observed. **C,D**. Freezing behavior measured in cued and contextual fear conditioning in *Gbx2Cre; Shox2KO* mice. No significant differences in freezing behavior to the context or cue were observed.

Acknowledgements: Funding NIH grants R21NS101482 to LAS and R01 HL136326 to YPC.

Authorship statement: DY and MM conceived experimental design, performed experiments, and wrote the manuscript. YS, XH, IF, CN, EM, SR contributed data. CS, WY (posthumous) contributed to early planning stages. YPC provided animals and reagents and LAS contributed to overall design and wrote manuscript.

bioRxiv preprint doi: https://doi.org/10.1101/660662; this version posted June 5, 2019. The copyright holder for this preprint (which was not certified by peer review) is the author/funder. All rights reserved. No reuse allowed without permission.

References:

1. Bal, T. & McCormick, D.A. What stops synchronized thalamocortical oscillations? *Neuron* **17**, 297-308 (1996).
2. Kim, J.H., Kim, J.B., Seo, W.K., Suh, S.I. & Koh, S.B. Volumetric and shape analysis of thalamus in idiopathic generalized epilepsy. *J Neurol* **260**, 1846-1854 (2013).
3. Williams, D. The thalamus and epilepsy. *Brain : a journal of neurology* **88**, 539-556 (1965).
4. Mory, S.B. *et al.* Structural abnormalities of the thalamus in juvenile myoclonic epilepsy. *Epilepsy & behavior : E&B* **21**, 407-411 (2011).
5. Nair, A., Treiber, J.M., Shukla, D.K., Shih, P. & Muller, R.A. Impaired thalamocortical connectivity in autism spectrum disorder: a study of functional and anatomical connectivity. *Brain : a journal of neurology* **136**, 1942-1955 (2013).
6. Tsatsanis, K.D. *et al.* Reduced thalamic volume in high-functioning individuals with autism. *Biol Psychiatry* **53**, 121-129 (2003).
7. Muller, R.A. *et al.* Underconnected, but how? A survey of functional connectivity MRI studies in autism spectrum disorders. *Cerebral cortex* **21**, 2233-2243 (2011).
8. Andreasen, N.C. The role of the thalamus in schizophrenia. *Can J Psychiatry* **42**, 27-33 (1997).
9. Brickman, A.M. *et al.* Thalamus size and outcome in schizophrenia. *Schizophr Res* **71**, 473-484 (2004).
10. Pinault, D. Dysfunctional thalamus-related networks in schizophrenia. *Schizophr Bull* **37**, 238-243 (2011).
11. Woodward, N.D., Karbasforoushan, H. & Heckers, S. Thalamocortical dysconnectivity in schizophrenia. *Am J Psychiatry* **169**, 1092-1099 (2012).
12. Warren, J.D., Thompson, P.D. & Thompson, P.D. Diencephalic amnesia and apraxia after left thalamic infarction. *J Neurol Neurosurg Psychiatry* **68**, 248 (2000).
13. Van der Werf, Y.D., Jolles, J., Witter, M.P. & Uylings, H.B. Contributions of thalamic nuclei to declarative memory functioning. *Cortex* **39**, 1047-1062 (2003).
14. Thielen, J.W., Takashima, A., Rutters, F., Tendolkar, I. & Fernandez, G. Transient relay function of midline thalamic nuclei during long-term memory consolidation in humans. *Learning & memory* **22**, 527-531 (2015).
15. Graff-Radford, N.R., Tranel, D., Van Hoesen, G.W. & Brandt, J.P. Diencephalic amnesia. *Brain : a journal of neurology* **113 (Pt 1)**, 1-25 (1990).
16. Garden, D.L. *et al.* Anterior thalamic lesions stop synaptic plasticity in retrosplenial cortex slices: expanding the pathology of diencephalic amnesia. *Brain : a journal of neurology* **132**, 1847-1857 (2009).
17. Dzieciol, A.M. *et al.* Hippocampal and diencephalic pathology in developmental amnesia. *Cortex* **86**, 33-44 (2017).
18. Llinas, R. & Jahnsen, H. Electrophysiology of mammalian thalamic neurones in vitro. *Nature* **297**, 406-408 (1982).
19. Jahnsen, H. & Llinas, R. Ionic basis for the electro-responsiveness and oscillatory properties of guinea-pig thalamic neurones in vitro. *The Journal of physiology* **349**, 227-247 (1984).
20. Deschenes, M., Paradis, M., Roy, J.P. & Steriade, M. Electrophysiology of neurons of lateral thalamic nuclei in cat: resting properties and burst discharges. *Journal of neurophysiology* **51**, 1196-1219 (1984).
21. McCormick, D.A. & Bal, T. Sleep and arousal: thalamocortical mechanisms. *Annual review of neuroscience* **20**, 185-215 (1997).
22. Clement-Jones, M. *et al.* The short stature homeobox gene SHOX is involved in skeletal abnormalities in Turner syndrome. *Human molecular genetics* **9**, 695-702 (2000).
23. De Baere, E., Speleman, F., Van Roy, N., De Paepe, A. & Messiaen, L. Assignment of SHOX2 (alias OG12X and SHOT) to human chromosome bands 3q25-->q26.1 by in situ hybridization. *Cytogenetics and cell*

bioRxiv preprint doi: https://doi.org/10.1101/660662; this version posted June 5, 2019. The copyright holder for this preprint (which was not certified by peer review) is the author/funder. All rights reserved. No reuse allowed without permission.

genetics **82**, 228-229 (1998).

24. Sun, C., Zhang, T., Liu, C., Gu, S. & Chen, Y. Generation of Shox2-Cre allele for tissue specific manipulation of genes in the developing heart, palate, and limb. *Genesis* **51**, 515-522 (2013).
25. Greisas, A. & Zlochiver, S. Modulation of cardiac pacemaker inter beat intervals by sinoatrial fibroblasts -a numerical study. *Conf Proc IEEE Eng Med Biol Soc* **2016**, 165-168 (2016).
26. Cribbs, L. T-type calcium channel expression and function in the diseased heart. *Channels (Austin)* **4**, 447-452 (2010).
27. Ludwig, A. *et al.* Absence epilepsy and sinus dysrhythmia in mice lacking the pacemaker channel HCN2. *The EMBO journal* **22**, 216-224 (2003).
28. Sun, C. *et al.* The short stature homeobox 2 (Shox2)-bone morphogenetic protein (BMP) pathway regulates dorsal mesenchymal protrusion development and its temporary function as a pacemaker during cardiogenesis. *The Journal of biological chemistry* **290**, 2007-2023 (2015).
29. Ye, W. *et al.* A common Shox2-Nkx2-5 antagonistic mechanism primes the pacemaker cell fate in the pulmonary vein myocardium and sinoatrial node. *Development* **142**, 2521-2532 (2015).
30. Ionta, V. *et al.* SHOX2 overexpression favors differentiation of embryonic stem cells into cardiac pacemaker cells, improving biological pacing ability. *Stem cell reports* **4**, 129-142 (2015).
31. Wang, J. *et al.* Pitx2 prevents susceptibility to atrial arrhythmias by inhibiting left-sided pacemaker specification. *Proceedings of the National Academy of Sciences of the United States of America* **107**, 9753-9758 (2010).
32. Rosin, J.M., Kurrasch, D.M. & Cobb, J. Shox2 is required for the proper development of the facial motor nucleus and the establishment of the facial nerves. *BMC neuroscience* **16**, 39 (2015).
33. Rosin, J.M. *et al.* Mice lacking the transcription factor SHOX2 display impaired cerebellar development and deficits in motor coordination. *Developmental biology* **399**, 54-67 (2015).
34. Dougherty, K.J. *et al.* Locomotor rhythm generation linked to the output of spinal shox2 excitatory interneurons. *Neuron* **80**, 920-933 (2013).
35. Abdo, H. *et al.* Dependence on the transcription factor Shox2 for specification of sensory neurons conveying discriminative touch. *The European journal of neuroscience* **34**, 1529-1541 (2011).
36. Ha, N.T. & Dougherty, K.J. Spinal Shox2 interneuron interconnectivity related to function and development. *Elife* **7** (2018).
37. Soriano, P. Generalized lacZ expression with the ROSA26 Cre reporter strain. *Nat Genet* **21**, 70-71 (1999).
38. Patro, R., Duggal, G., Love, M.I., Irizarry, R.A. & Kingsford, C. Salmon provides fast and bias-aware quantification of transcript expression. *Nat Methods* **14**, 417-419 (2017).
39. Love, M.I., Huber, W. & Anders, S. Moderated estimation of fold change and dispersion for RNA-seq data with DESeq2. *Genome Biol* **15**, 550 (2014).
40. Huang da, W., Sherman, B.T. & Lempicki, R.A. Systematic and integrative analysis of large gene lists using DAVID bioinformatics resources. *Nat Protoc* **4**, 44-57 (2009).
41. Huang da, W., Sherman, B.T. & Lempicki, R.A. Bioinformatics enrichment tools: paths toward the comprehensive functional analysis of large gene lists. *Nucleic acids research* **37**, 1-13 (2009).
42. Valente, V. *et al.* Selection of suitable housekeeping genes for expression analysis in glioblastoma using quantitative RT-PCR. *BMC molecular biology* **10**, 17 (2009).
43. Li, B. *et al.* Identification of optimal reference genes for RT-qPCR in the rat hypothalamus and intestine for the study of obesity. *Int J Obes (Lond)* **38**, 192-197 (2014).
44. Puil, E., Gimbarzevsky, B. & Miura, R.M. Quantification of membrane properties of trigeminal root ganglion neurons in guinea pigs. *Journal of neurophysiology* **55**, 995-1016 (1986).
45. Zhang, C., Bosch, M.A., Rick, E.A., Kelly, M.J. & Ronnekleiv, O.K. 17Beta-estradiol regulation of T-type calcium channels in gonadotropin-releasing hormone neurons. *The Journal of neuroscience : the official journal of the Society for Neuroscience* **29**, 10552-10562 (2009).

bioRxiv preprint doi: https://doi.org/10.1101/660662; this version posted June 5, 2019. The copyright holder for this preprint (which was not certified by peer review) is the author/funder. All rights reserved. No reuse allowed without permission.

46. Bhattacharjee, A., Whitehurst, R.M., Jr., Zhang, M., Wang, L. & Li, M. T-type calcium channels facilitate insulin secretion by enhancing general excitability in the insulin-secreting beta-cell line, INS-1. *Endocrinology* **138**, 3735-3740 (1997).
47. Lee, J.H., Gomora, J.C., Cribbs, L.L. & Perez-Reyes, E. Nickel block of three cloned T-type calcium channels: low concentrations selectively block alpha1H. *Biophysical journal* **77**, 3034-3042 (1999).
48. Antunes, M. & Biala, G. The novel object recognition memory: neurobiology, test procedure, and its modifications. *Cogn Process* **13**, 93-110 (2012).
49. Arakawa, H. *et al.* Thalamic NMDA receptor function is necessary for patterning of the thalamocortical somatosensory map and for sensorimotor behaviors. *The Journal of neuroscience : the official journal of the Society for Neuroscience* **34**, 12001-12014 (2014).
50. Can, A. *et al.* The mouse forced swim test. *J Vis Exp*, e3638 (2012).
51. Gusel'nikova, V.V. & Korzhevskiy, D.E. NeuN As a Neuronal Nuclear Antigen and Neuron Differentiation Marker. *Acta Naturae* **7**, 42-47 (2015).
52. Herculano-Houzel, S. & Lent, R. Isotropic fractionator: a simple, rapid method for the quantification of total cell and neuron numbers in the brain. *The Journal of neuroscience : the official journal of the Society for Neuroscience* **25**, 2518-2521 (2005).
53. Eng, L.F. Glial fibrillary acidic protein (GFAP): the major protein of glial intermediate filaments in differentiated astrocytes. *J Neuroimmunol* **8**, 203-214 (1985).
54. Yang, Z. & Wang, K.K. Glial fibrillary acidic protein: from intermediate filament assembly and gliosis to neurobiomarker. *Trends in neurosciences* **38**, 364-374 (2015).
55. Arcelli, P., Frassoni, C., Regondi, M.C., De Biasi, S. & Spreafico, R. GABAergic neurons in mammalian thalamus: a marker of thalamic complexity? *Brain research bulletin* **42**, 27-37 (1997).
56. Song, I. *et al.* Role of the alpha1G T-type calcium channel in spontaneous absence seizures in mutant mice. *The Journal of neuroscience : the official journal of the Society for Neuroscience* **24**, 5249-5257 (2004).
57. Kim, D. *et al.* Lack of the burst firing of thalamocortical relay neurons and resistance to absence seizures in mice lacking alpha(1G) T-type Ca(2+) channels. *Neuron* **31**, 35-45 (2001).
58. Zhang, Y., Vilaythong, A.P., Yoshor, D. & Noebels, J.L. Elevated thalamic low-voltage-activated currents precede the onset of absence epilepsy in the SNAP25-deficient mouse mutant coloboma. *The Journal of neuroscience : the official journal of the Society for Neuroscience* **24**, 5239-5248 (2004).
59. Talley, E.M. *et al.* Differential distribution of three members of a gene family encoding low voltage-activated (T-type) calcium channels. *The Journal of neuroscience : the official journal of the Society for Neuroscience* **19**, 1895-1911 (1999).
60. Kim, D. *et al.* Lack of the burst firing of thalamocortical relay neurons and resistance to absence seizures in mice lacking alpha(1G) T-type Ca(2+) channels

Neuron **31**, 35-45 (2001).
61. Anderson, M.P. *et al.* Thalamic Cav3.1 T-type Ca2+ channel plays a crucial role in stabilizing sleep. *Proceedings of the National Academy of Sciences of the United States of America* **102**, 1743-1748 (2005).
62. Moosmang, S., Biel, M., Hofmann, F. & Ludwig, A. Differential distribution of four hyperpolarization-activated cation channels in mouse brain. *Biological chemistry* **380**, 975-980 (1999).
63. Llinas, R.R. & Steriade, M. Bursting of thalamic neurons and states of vigilance. *Journal of neurophysiology* **95**, 3297-3308 (2006).
64. Puil, E., Meiri, H. & Yarom, Y. Resonant behavior and frequency preferences of thalamic neurons. *Journal of neurophysiology* **71**, 575-582 (1994).
65. Hutcheon, B., Miura, R.M., Yarom, Y. & Puil, E. Low-threshold calcium current and resonance in thalamic neurons: a model of frequency preference. *Journal of neurophysiology* **71**, 583-594 (1994).

bioRxiv preprint doi: https://doi.org/10.1101/660662; this version posted June 5, 2019. The copyright holder for this preprint (which was not certified by peer review) is the author/funder. All rights reserved. No reuse allowed without permission.

66. Hutcheon, B. & Yarom, Y. Resonance, oscillation and the intrinsic frequency preferences of neurons. *Trends in neurosciences* **23**, 216-222 (2000).
67. Xue, W.N. *et al.* SK- and h-current contribute to the generation of theta-like resonance of rat substantia nigra pars compacta dopaminergic neurons at hyperpolarized membrane potentials. *Brain Struct Funct* **217**, 379-394 (2012).
68. Hu, H., Vervaeke, K. & Storm, J.F. Two forms of electrical resonance at theta frequencies, generated by M-current, h-current and persistent Na+ current in rat hippocampal pyramidal cells. *The Journal of physiology* **545**, 783-805 (2002).
69. Williams, S.R., Toth, T.I., Turner, J.P., Hughes, S.W. & Crunelli, V. The 'window' component of the low threshold Ca2+ current produces input signal amplification and bistability in cat and rat thalamocortical neurones. *The Journal of physiology* **505 (Pt 3)**, 689-705 (1997).
70. Hughes, S.W., Cope, D.W., Toth, T.I., Williams, S.R. & Crunelli, V. All thalamocortical neurones possess a T-type Ca2+ 'window' current that enables the expression of bistability-mediated activities. *The Journal of physiology* **517 (Pt 3)**, 805-815 (1999).
71. Crunelli, V., Toth, T.I., Cope, D.W., Blethyn, K. & Hughes, S.W. The 'window' T-type calcium current in brain dynamics of different behavioural states. *The Journal of physiology* **562**, 121-129 (2005).
72. Crunelli, V., Cope, D.W. & Hughes, S.W. Thalamic T-type Ca2+ channels and NREM sleep. *Cell calcium* **40**, 175-190 (2006).
73. Dreyfus, F.M. *et al.* Selective T-type calcium channel block in thalamic neurons reveals channel redundancy and physiological impact of I(T)window. *The Journal of neuroscience : the official journal of the Society for Neuroscience* **30**, 99-109 (2010).
74. Zobeiri, M. *et al.* Modulation of thalamocortical oscillations by TRIP8b, an auxiliary subunit for HCN channels. *Brain Struct Funct* (2017).
75. Zobeiri, M. *et al.* The Hyperpolarization-Activated HCN4 Channel is Important for Proper Maintenance of Oscillatory Activity in the Thalamocortical System. *Cerebral cortex* (2019).
76. Mallika, C., Guo, Q. & Li, J.Y. Gbx2 is essential for maintaining thalamic neuron identity and repressing habenular characters in the developing thalamus. *Developmental biology* **407**, 26-39 (2015).
77. Chen, L., Guo, Q. & Li, J.Y. Transcription factor Gbx2 acts cell-nonautonomously to regulate the formation of lineage-restriction boundaries of the thalamus. *Development* **136**, 1317-1326 (2009).
78. Seibenhener, M.L. & Wooten, M.C. Use of the Open Field Maze to measure locomotor and anxiety-like behavior in mice. *J Vis Exp*, e52434 (2015).
79. Castagne, V., Moser, P., Roux, S. & Porsolt, R.D. Rodent models of depression: forced swim and tail suspension behavioral despair tests in rats and mice. *Curr Protoc Neurosci* **Chapter 8**, Unit 8 10A (2011).
80. Jankowski, M.M. *et al.* The anterior thalamus provides a subcortical circuit supporting memory and spatial navigation. *Frontiers in systems neuroscience* **7**, 45 (2013).
81. Aggleton, J.P. & Sahgal, A. The contribution of the anterior thalamic nuclei to anterograde amnesia. *Neuropsychologia* **31**, 1001-1019 (1993).
82. Aggleton, J.P. & Mishkin, M. Memory impairments following restricted medial thalamic lesions in monkeys. *Experimental brain research* **52**, 199-209 (1983).
83. Aggleton, J.P., Dumont, J.R. & Warburton, E.C. Unraveling the contributions of the diencephalon to recognition memory: a review. *Learning & memory* **18**, 384-400 (2011).
84. Vogel-Ciernia, A. & Wood, M.A. Examining object location and object recognition memory in mice. *Curr Protoc Neurosci* **69**, 8 31 31-17 (2014).
85. Murai, T., Okuda, S., Tanaka, T. & Ohta, H. Characteristics of object location memory in mice: Behavioral and pharmacological studies. *Physiology & behavior* **90**, 116-124 (2007).
86. Padilla-Coreano, N., Do-Monte, F.H. & Quirk, G.J. A time-dependent role of midline thalamic nuclei in the retrieval of fear memory. *Neuropharmacology* **62**, 457-463 (2012).

bioRxiv preprint doi: https://doi.org/10.1101/660662; this version posted June 5, 2019. The copyright holder for this preprint (which was not certified by peer review) is the author/funder. All rights reserved. No reuse allowed without permission.

87. Dumont, J.R. & Aggleton, J.P. Dissociation of recognition and recency memory judgments after anterior thalamic nuclei lesions in rats. *Behavioral neuroscience* **127**, 415-431 (2013).
88. Powell, A.L. *et al.* The retrosplenial cortex and object recency memory in the rat. *The European journal of neuroscience* **45**, 1451-1464 (2017).
89. Elijah, D.H., Samengo, I. & Montemurro, M.A. Thalamic neuron models encode stimulus information by burst-size modulation. *Front Comput Neurosci* **9**, 113 (2015).
90. Sherman, S.M. Dual response modes in lateral geniculate neurons: mechanisms and functions. *Vis Neurosci* **13**, 205-213 (1996).
91. McCormick, D.A. & Pape, H.C. Properties of a hyperpolarization-activated cation current and its role in rhythmic oscillation in thalamic relay neurones. *The Journal of physiology* **431**, 291-318 (1990).
92. McCormick, D.A. & Feeser, H.R. Functional implications of burst firing and single spike activity in lateral geniculate relay neurons. *Neuroscience* **39**, 103-113 (1990).
93. Jeanmonod, D., Magnin, M. & Morel, A. Low-threshold calcium spike bursts in the human thalamus. Common physiopathology for sensory, motor and limbic positive symptoms. *Brain : a journal of neurology* **119 (Pt 2)**, 363-375 (1996).
94. Guillery, R.W. & Sherman, S.M. Thalamic relay functions and their role in corticocortical communication: generalizations from the visual system. *Neuron* **33**, 163-175 (2002).
95. Sherman, S.M. & Guillery, R.W. The role of the thalamus in the flow of information to the cortex. *Philos Trans R Soc Lond B Biol Sci* **357**, 1695-1708 (2002).
96. Sherman, S.M. & Guillery, R.W. Functional organization of thalamocortical relays. *Journal of neurophysiology* **76**, 1367-1395 (1996).
97. Sherman, S.M. A wake-up call from the thalamus. *Nature neuroscience* **4**, 344-346 (2001).
98. Reinagel, P., Godwin, D., Sherman, S.M. & Koch, C. Encoding of visual information by LGN bursts. *Journal of neurophysiology* **81**, 2558-2569 (1999).
99. Marlinski, V. & Beloozerova, I.N. Burst firing of neurons in the thalamic reticular nucleus during locomotion. *Journal of neurophysiology* **112**, 181-192 (2014).
100. Guido, W., Lu, S.M. & Sherman, S.M. Relative contributions of burst and tonic responses to the receptive field properties of lateral geniculate neurons in the cat. *Journal of neurophysiology* **68**, 2199-2211 (1992).
101. Zeldenrust, F., Wadman, W.J. & Englitz, B. Neural Coding With Bursts-Current State and Future Perspectives. *Front Comput Neurosci* **12**, 48 (2018).
102. Zeldenrust, F., Chameau, P. & Wadman, W.J. Spike and burst coding in thalamocortical relay cells. *PLoS Comput Biol* **14**, e1005960 (2018).
103. Liu, H. *et al.* The role of Shox2 in SAN development and function. *Pediatric cardiology* **33**, 882-889 (2012).
104. Liu, H. *et al.* Functional redundancy between human SHOX and mouse Shox2 genes in the regulation of sinoatrial node formation and pacemaking function. *The Journal of biological chemistry* **286**, 17029-17038 (2011).
105. Li, N. *et al.* A SHOX2 loss-of-function mutation underlying familial atrial fibrillation. *Int J Med Sci* **15**, 1564-1572 (2018).
106. Hoffmann, S. *et al.* Coding and non-coding variants in the SHOX2 gene in patients with early-onset atrial fibrillation. *Basic research in cardiology* **111**, 36 (2016).
107. Liu, H. *et al.* Phosphorylation of Shox2 is required for its function to control sinoatrial node formation. *Journal of the American Heart Association* **3**, e000796 (2014).
108. Nielsen, J. & Wohlert, M. Sex chromosome abnormalities found among 34,910 newborn children: results from a 13-year incidence study in Arhus, Denmark. *Birth Defects Orig Artic Ser* **26**, 209-223 (1990).
109. Jacobs, P. *et al.* Turner syndrome: a cytogenetic and molecular study. *Ann Hum Genet* **61**, 471-483 (1997).
110. Oliveira, C.S. & Alves, C. The role of the SHOX gene in the pathophysiology of Turner syndrome.

bioRxiv preprint doi: https://doi.org/10.1101/660662; this version posted June 5, 2019. The copyright holder for this preprint (which was not certified by peer review) is the author/funder. All rights reserved. No reuse allowed without permission.

Endocrinologia y nutricion : organo de la Sociedad Espanola de Endocrinologia y Nutricion **58**, 433-442 (2011).

111. Joseph, M. *et al.* Xp pseudoautosomal gene haploinsufficiency and linear growth deficiency in three girls with chromosome Xp22;Yq11 translocation. *Journal of medical genetics* **33**, 906-911 (1996).
112. Blaschke, R.J. *et al.* SHOT, a SHOX-related homeobox gene, is implicated in craniofacial, brain, heart, and limb development. *Proceedings of the National Academy of Sciences of the United States of America* **95**, 2406-2411 (1998).
113. Mauger, C. *et al.* Executive Functions in Children and Adolescents with Turner Syndrome: A Systematic Review and Meta-Analysis. *Neuropsychol Rev* **28**, 188-215 (2018).
114. Zhao, H. & Lian, Y.J. Epilepsy associated with Turner syndrome. *Neurol India* **63**, 631-633 (2015).
115. Saad, K. *et al.* Turner syndrome: review of clinical, neuropsychiatric, and EEG status: an experience of tertiary center. *Acta Neurol Belg* **114**, 1-9 (2014).
116. Puusepp, H., Zordania, R., Paal, M., Bartsch, O. & Ounap, K. Girl with partial Turner syndrome and absence epilepsy. *Pediatr Neurol* **38**, 289-292 (2008).
117. Magara, S. *et al.* Rub epilepsy in an infant with Turner syndrome. *Brain Dev* **37**, 725-728 (2015).
118. Jhang, K.M., Chang, T.M., Chen, M. & Liu, C.S. Generalized epilepsy in a patient with mosaic Turner syndrome: a case report. *J Med Case Rep* **8**, 109 (2014).
119. Knickmeyer, R.C. & Davenport, M. Turner syndrome and sexual differentiation of the brain: implications for understanding male-biased neurodevelopmental disorders. *J Neurodev Disord* **3**, 293-306 (2011).

Figure 1. Yu et. al.

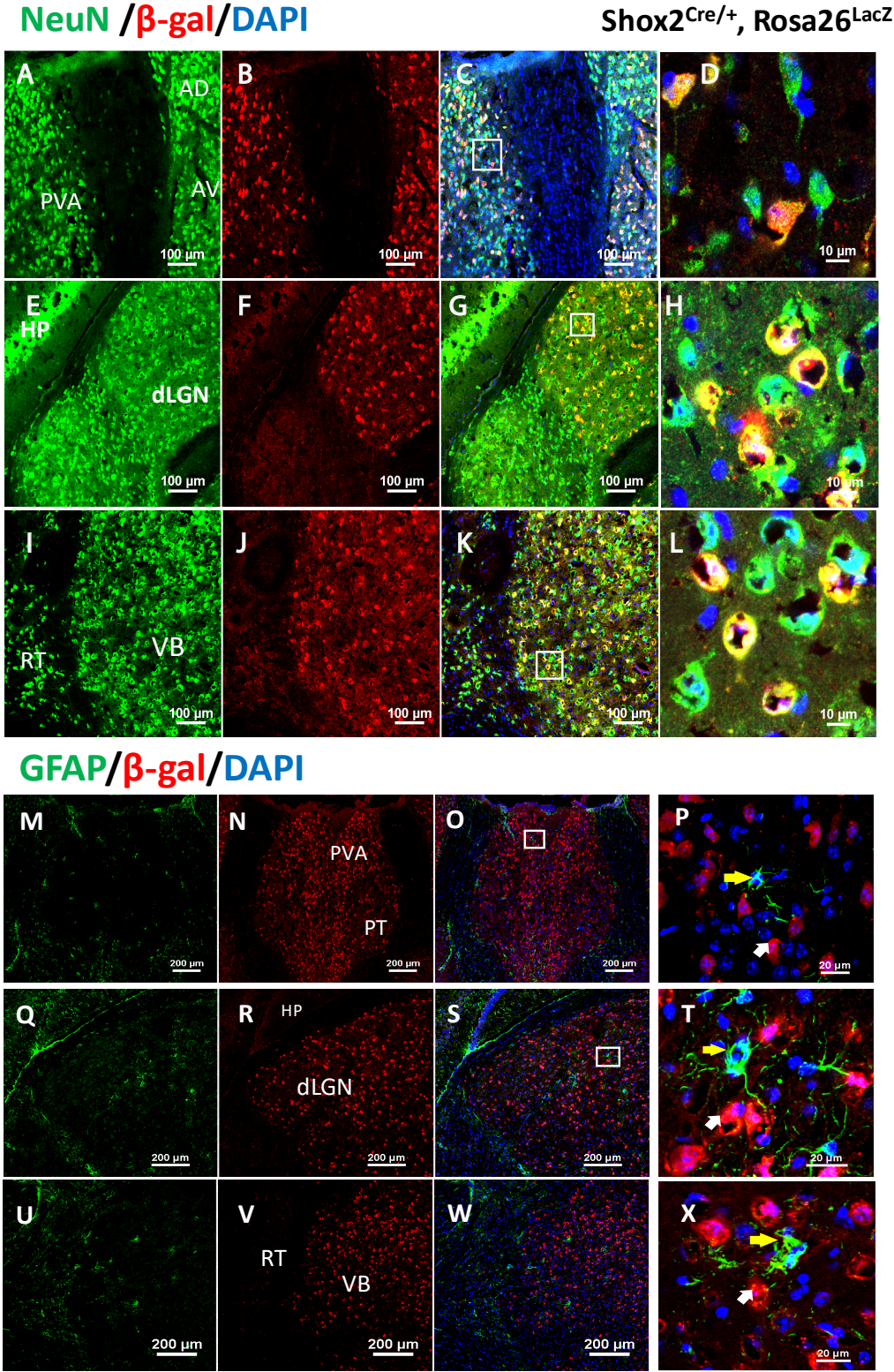

Figure 2. Yu et. al.

DAPI/PV/β-gal

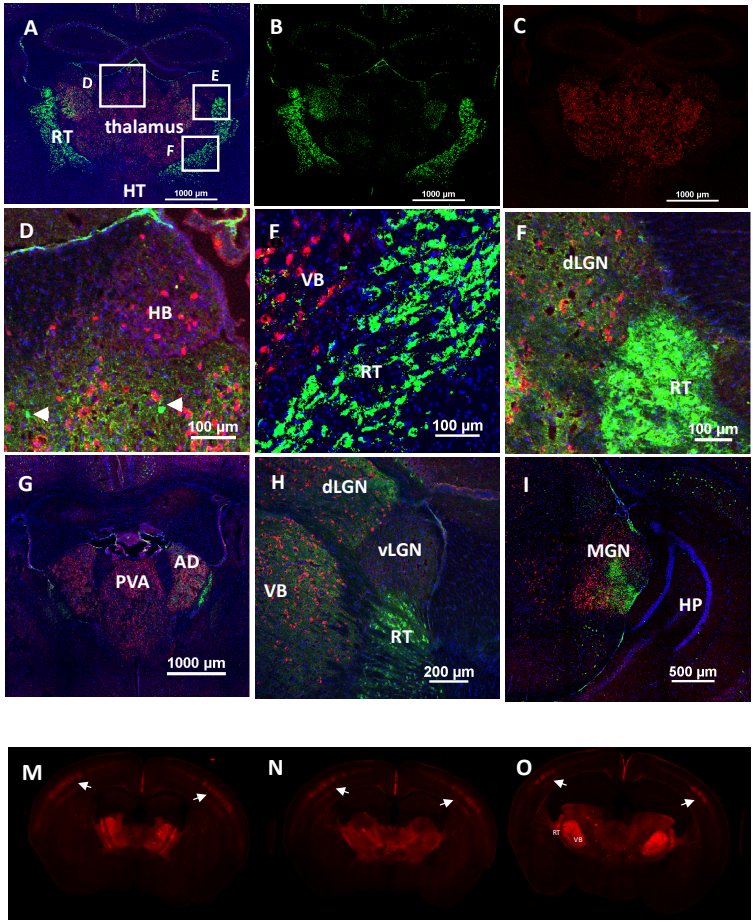

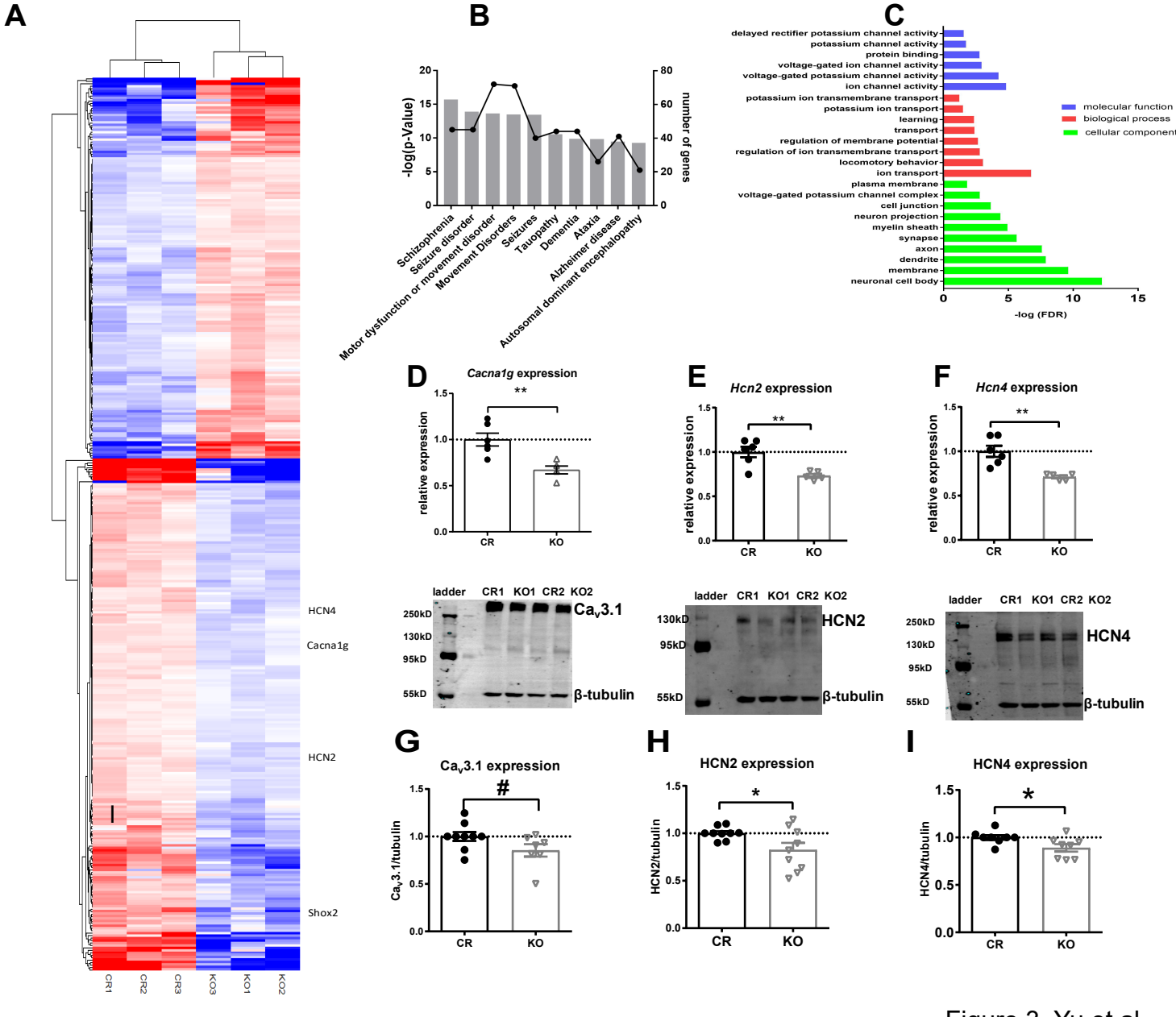

Figure 3. Yu et al

Figure 4. Yu et. al.

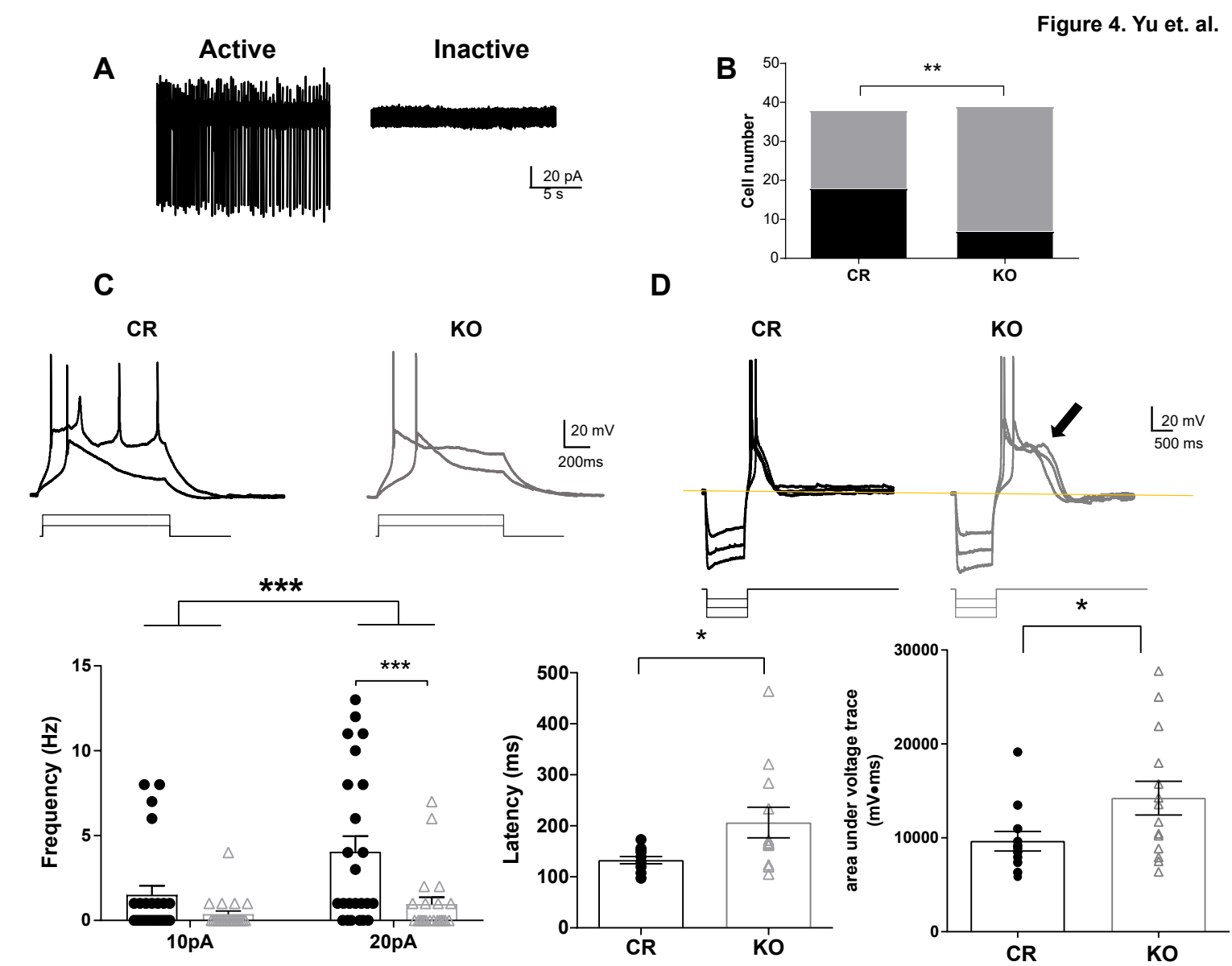

Figure 5. Yu et al.

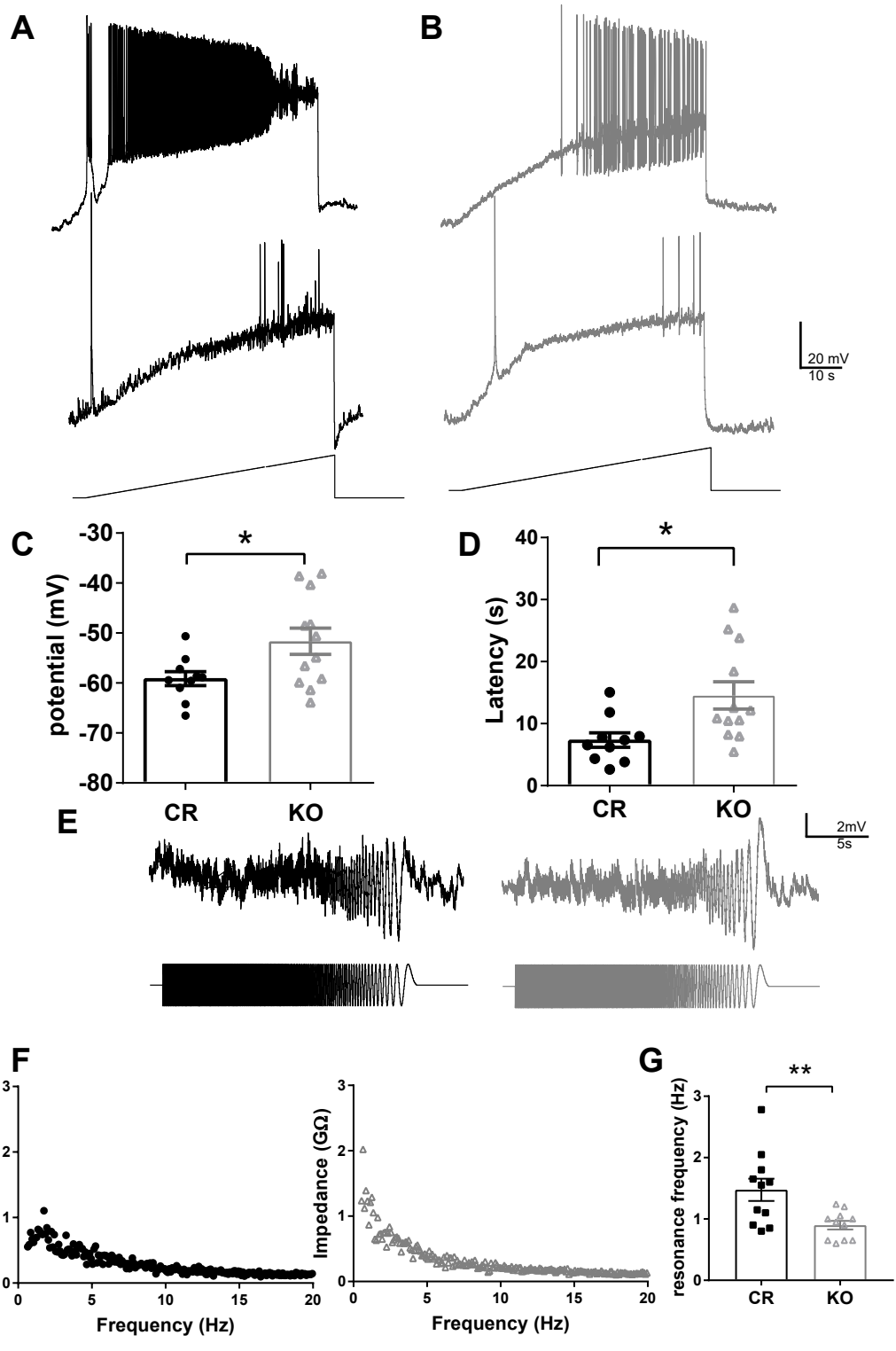

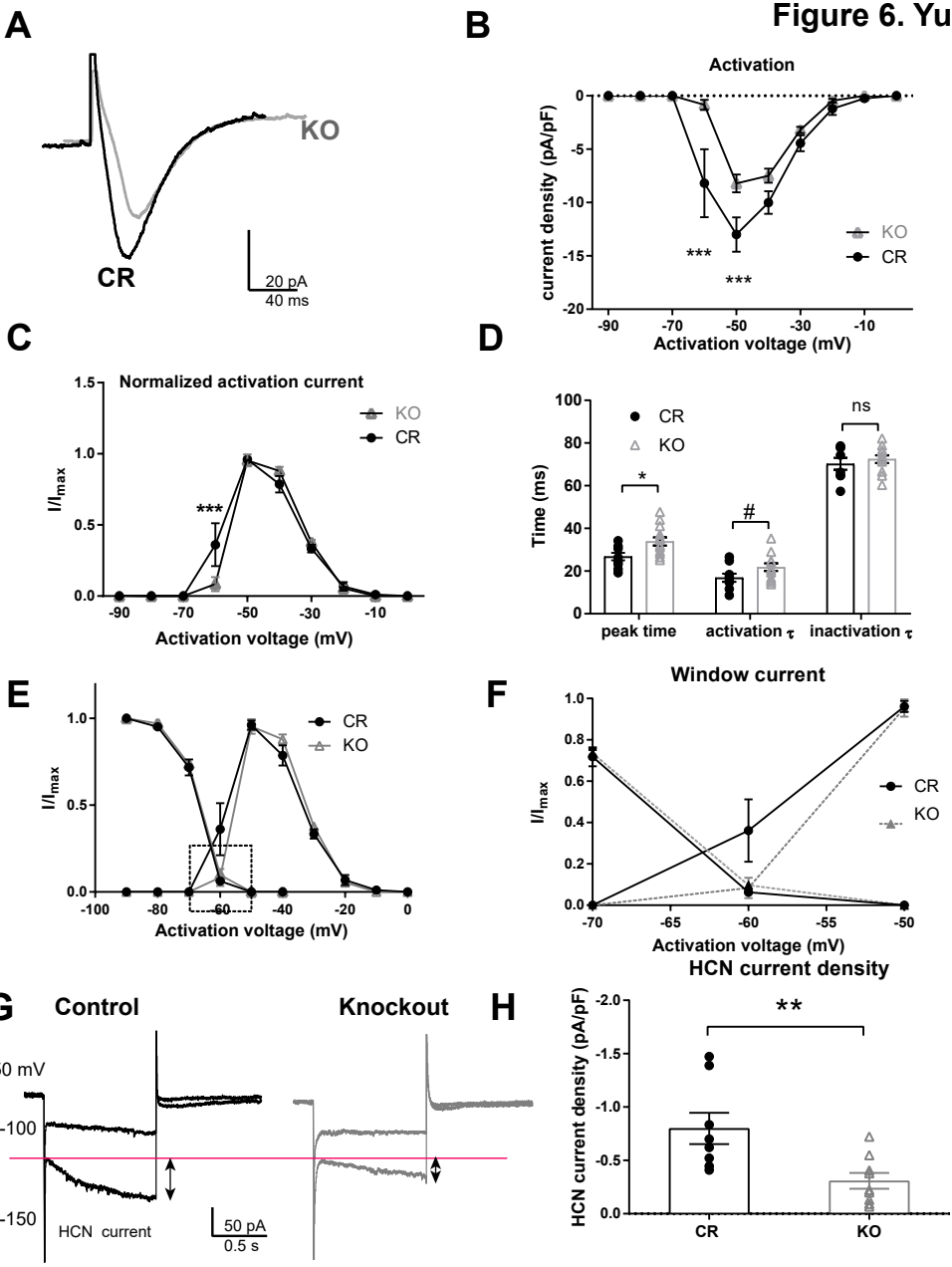
A
KO
CR
20 pA
40 ms
B
Activation
current density (pA/pF)
KO
CR
***
***
Activation voltage (mV)
C
Normalized activation current
I/Imax
KO
CR
***
Activation voltage (mV)
D
Time (ms)
CR
KO
*
#
ns
peak time
activation τ
inactivation τ
E
I/Imax
CR
KO
Activation voltage (mV)
F
Window current
I/Imax
CR
KO
Activation voltage (mV)
G
Control
Knockout
-50 mV
-100
-150
HCN current
50 pA
0.5 s
H
HCN current density
HCN current density (pA/pF)
**
CR
KO

Figure 7. Yu et. al.